

## Development of nanoparticles bulk morphology analysis: Multidomain XRD approach

Iliia Smirnov <sup>a\*</sup>, Zbigniew Kaszukur <sup>a\*</sup>, Armin Hoell <sup>b</sup>

<sup>a</sup> Institute of Physical Chemistry, Warsaw, Poland

<sup>b</sup> Helmholtz-Zentrum Berlin für Materialien und Energie, Germany

Correspondence and requests for materials should be addressed to I.S. (email: ismirnov@ichf.edu.pl) or Z.K. (email: zkaszukur@ichf.edu.pl)

### Supplementary Figures

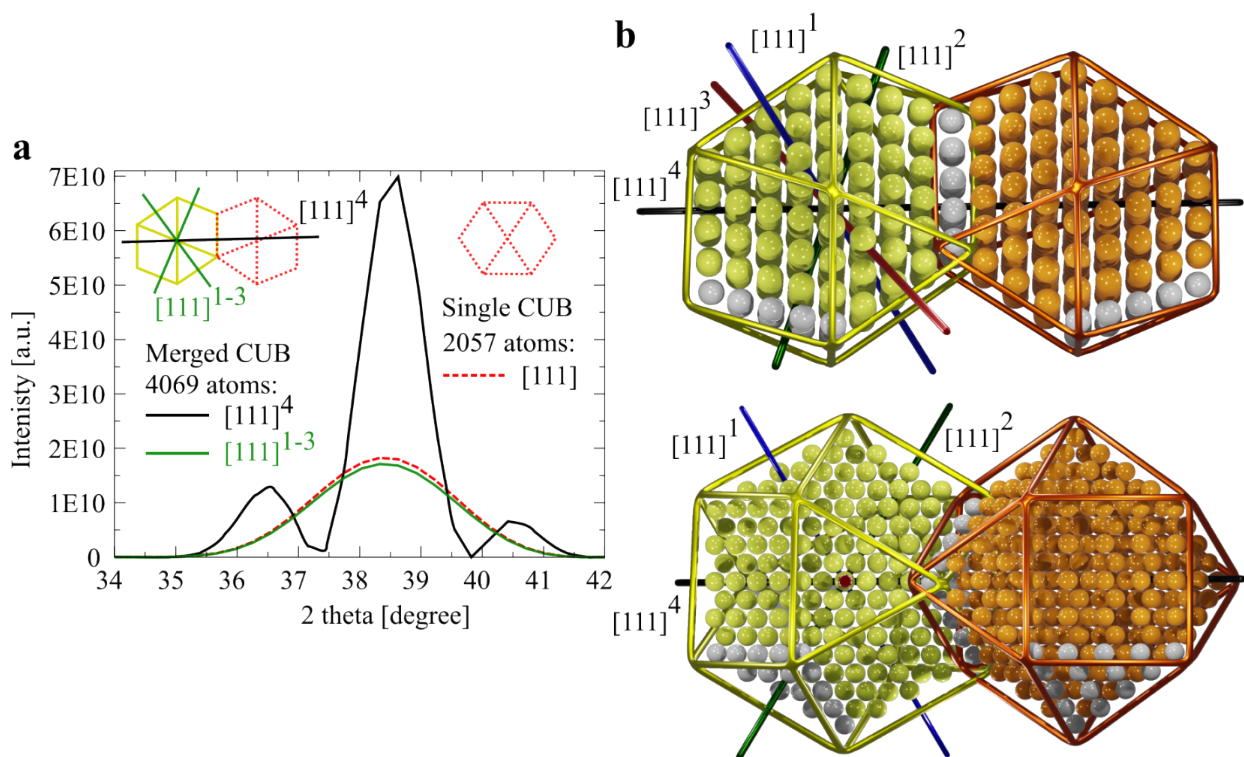


Figure S 1 (a) XRD crystal patterns of two merged CUBs oriented along  $[111]^3$  (black line shows extended  $[111]^4$  direction, blue, green and red lines represent other  $[111]^{1-3}$  directions) and of single CUB extracted from the merged model. The height of X-ray peak along  $[111]^4$  is  $\sim 3.88$  times greater than the height along  $[111]^{1-3}$ . The increment is smaller than predicted by equation 1 because two CUBs were merged by one 111 plane. Therefore, the length of extended  $[111]^4$  row of atoms is only nearly doubled (minus one atom belonging to the mirror plane). (b) The scheme of all  $[111]$  directions for the left CUB (shown by the yellow cage). Clusters shown on the picture

are two merged CUBs. The initial number of atoms in the single CUB equals 309. The merged CUBs model consists of 603 atoms.

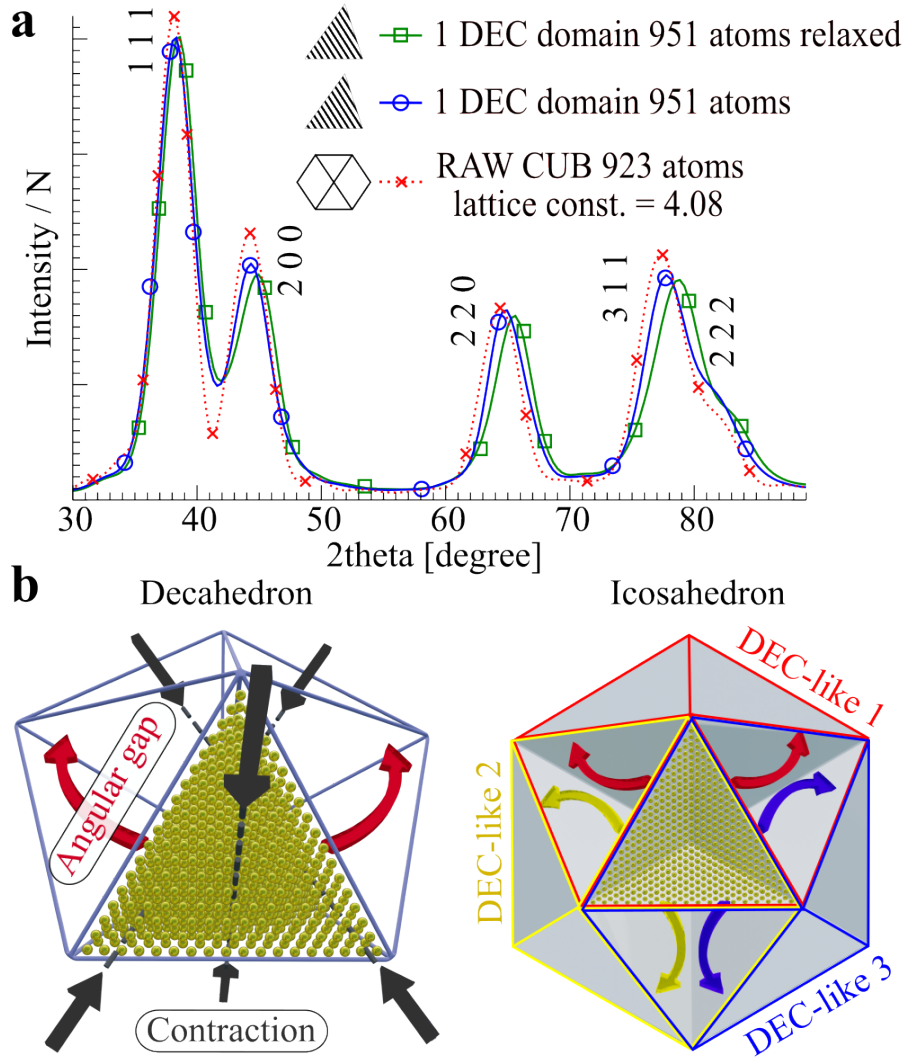
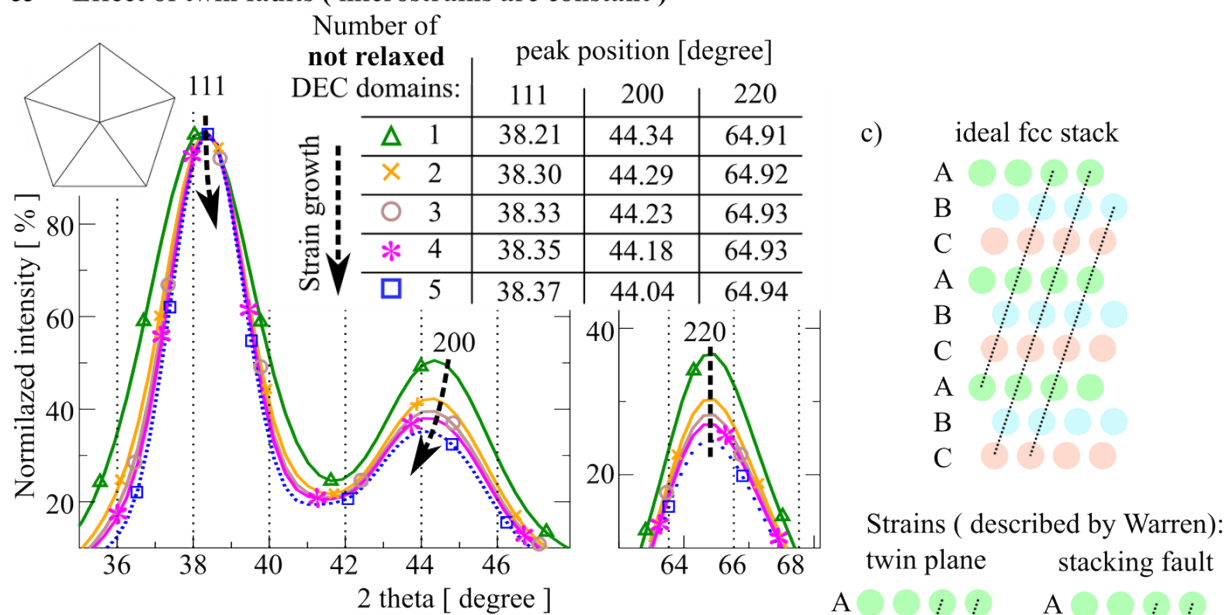


Figure S 2 (a) Comparison of XRD patterns of single non-relaxed and relaxed domains of the relaxed DEC structure; and of the non-relaxed, perfect fcc CUB model . 1 DEC domain model preserved strain of the original 4772 atom decahedron. After the relaxation all peaks were shifted to the right-hand side (contraction of the lattice). This observation shows existence of contraction forces within DEC. (b) Schematic representation of the forces acting on the lattice inside decahedron and icosahedron. Within ICO one may distinguish several 5-fold 5 domain DEC clusters (DEC-like 1,2,3). These DEC's have a common single domain what creates an extraordinary stress (mixture of contraction and expansion forces) on each domain.

**a Effect of twin faults ( microstrains are constant )**



**b Formation of microstrains + effect of twin faults**

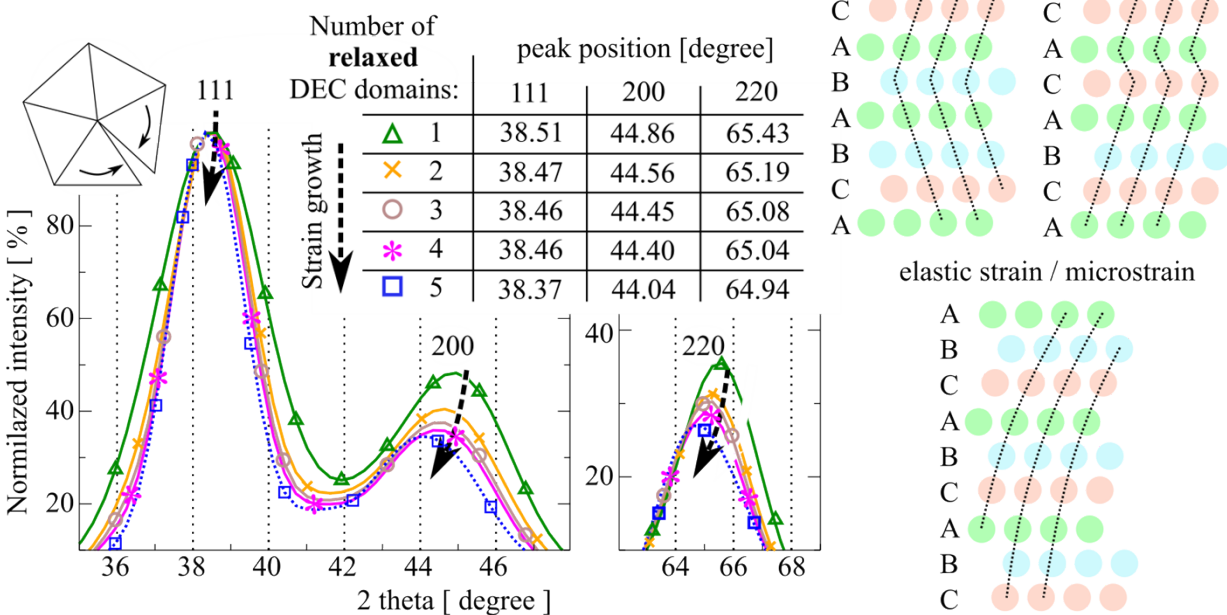


Figure S 3 (a) XRD patterns of non - relaxed DEC derivatives: 1 domain (green triangles), 2 neighbor domains (yellow crosses), 3 neighbor domains (brown circles), 4 domains (purple asterisks) and full decahedron (blue squares). (b) XRD patterns of relaxed DEC derivatives: 1 domain (green triangles), 2 neighbor domains (yellow crosses), 3 neighbor domains (brown circles), 4 domains (purple asterisks) and full decahedron (blue squares). (c) Schematic illustration: ideal fcc stacking defects, twin and stacking faults, elastic deformation (microstrain).

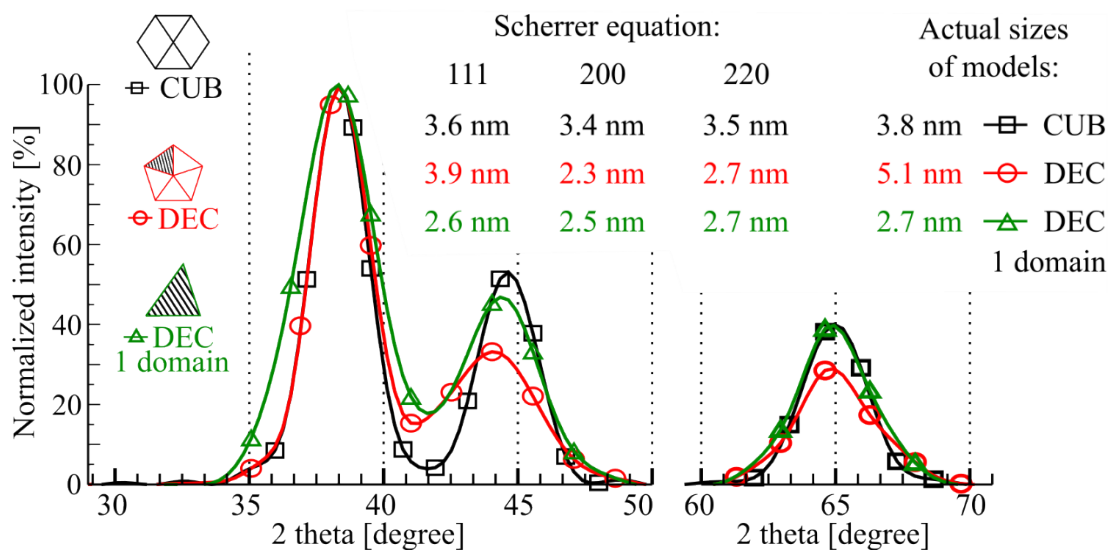


Figure S 4 Calculated XRD patterns of CUB with 2057 atoms (black squares), DEC with 4776 atoms (red circles), 1 DEC domain with 951 atoms (green triangles). 1 DEC domain was relaxed. The peak heights of the relaxed 1 DEC domain are similar to that of the CUB pattern. However, 200 peak heights of 1 DEC domain and CUB are different, because the 200 peak is sensitive to shape of the domain (Figure S 7) and to the strain <sup>1</sup>.

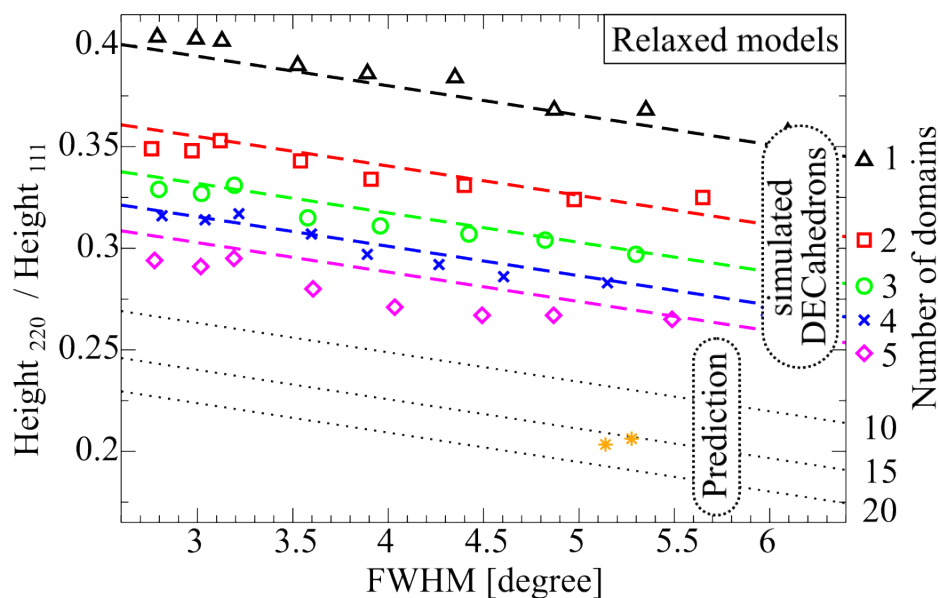


Figure S 5  $H_{220}/H_{111}$  ratio as a function of 220 peak FWHM. 10 relaxed gold DEC models were separated into 1-5 domain structures. The yellow stars represent ICO models with 12431 and with 14993 atoms.

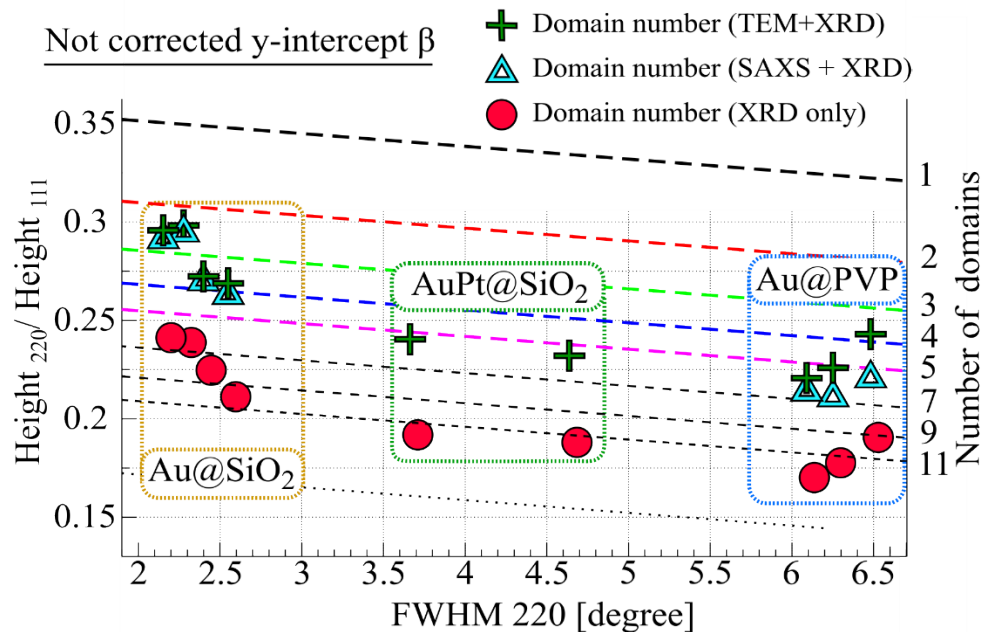


Figure S 6 Domain number analysis of experimental samples by three different methods (x-scale from XRD): MDXRD method - left y axis (red circles); a combination of TEM (a mean volume-weighted size) and XRD (shown by green pluses); a combination of SAXS mean size analysis (volume-weighted fraction) and XRD (shown in blue triangles). All combined methods use right hand y-axis and equation 5 supplying 'actual size' from the used method.

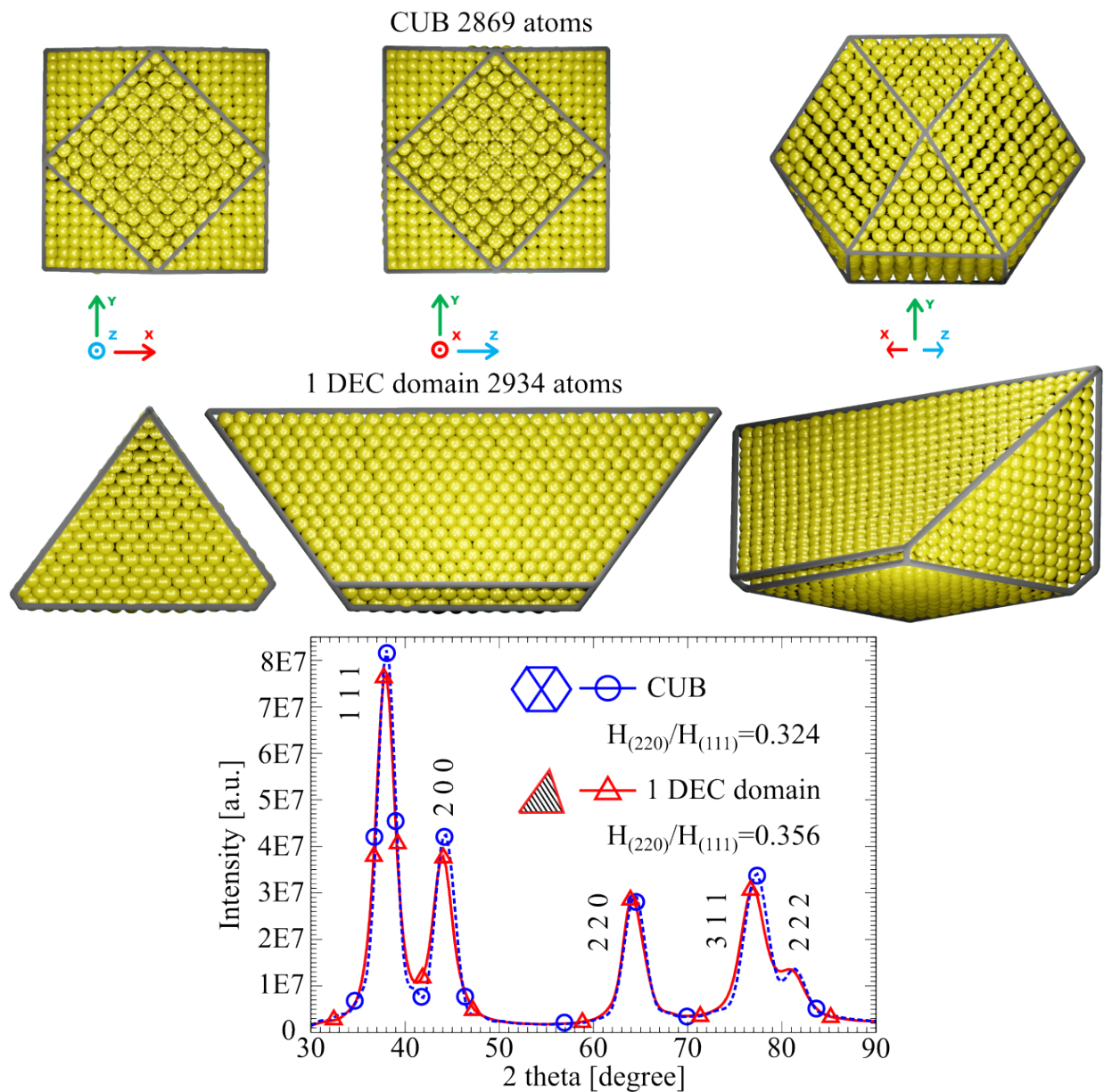


Figure S 7 Calculated XRD patterns of CUB (2869 atoms) and 1 (Marks) DEC domain (2934 atoms). Both models were subjected to molecular dynamics simulation at 293 K for at least 30 psec. The shape of models is different, therefore the lengths of atom rows in various crystallographic directions are also different. Although the lengths in [220] directions are equivalent (the same height for the CUB and 1 domain DEC models), it is not so for [111] directions. This causes decrease of 111 peak height. Therefore the  $H_{220}/H_{111}$  ratio of 1 DEC domain is greater than for CUB model.

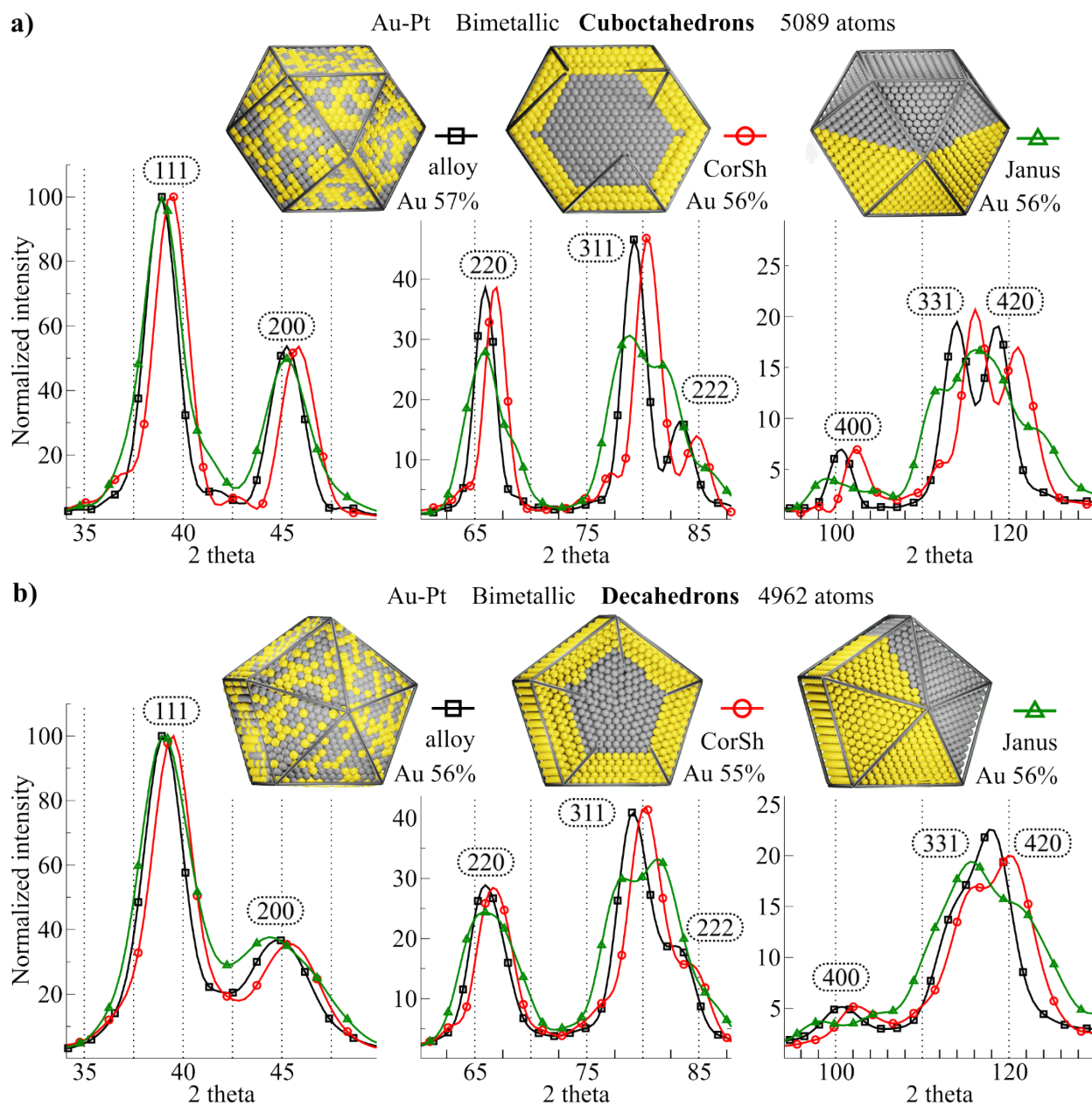


Figure S 8 Calculated X-ray diffraction patterns of relaxed Au-Pt nanoparticles: a) cuboctahedron particles (5089 atoms); b) Marks DEC ( $m=13$ ,  $n=9$ ,  $p=1$ ) particles (4962 atoms). All patterns were normalized by equalizing the height of 111 peaks.

Both alloyed and core-shell nanoparticles (regardless of the type of morphology) have almost the same  $H_{220}/H_{111}$  ratio and peak widths. Therefore, MDXRD applied to these NPs will provide the same (correct) results. These particular simulations show that the multidomain approach can be applied for the analysis of core-shell structure with similar lattice constants (for example, for Au and Pt).

However, the wide applicability of MDXRD to core-shell structures needs to be further justified. If the core-shell structure is highly strained, this can cause a change in the  $H_{220}/H_{111}$  ratio and a significant broadening of the 220 peak. As a result, MDXRD will contain significant error.

As it can be seen from the figure above, the multidomain approach is not applicable to Janus nanoparticles. In the case of these structures (even for very large ones with a size of  $\sim 10$  nm), there is no clear phase separation of the 111 peak. Therefore, there is no way to evaluate heights of 111 peaks of Au and Pt. Despite the fact, that 220 peaks indicate phase separation, it is still difficult to separate the Au and Pt contributions. In the case of real samples, it will be even more difficult. Therefore, it is impossible to determine properly 220 peaks parameters for Au and Pt lobes separately. Since key parameters of the multidomain approach cannot be determined, this method cannot be applied to Janus structures.

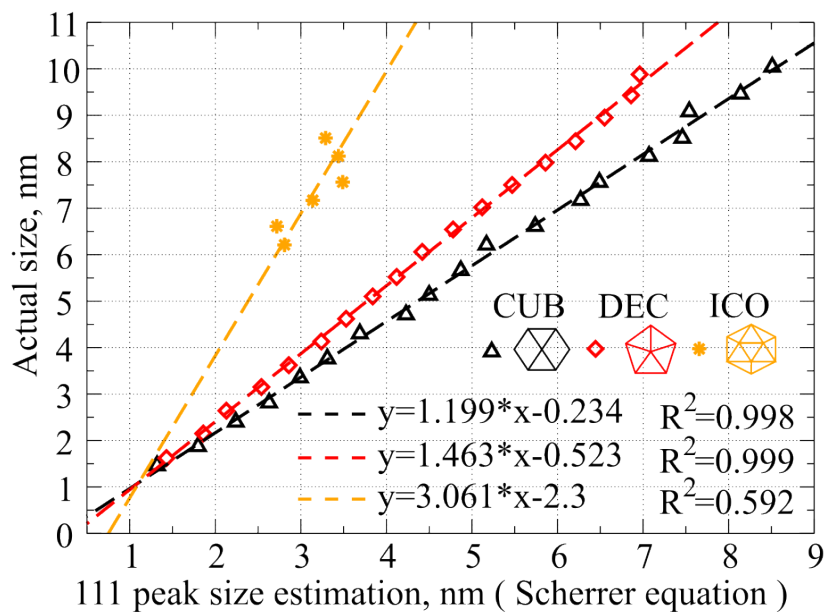


Figure S 9 The dependence of a real cluster size versus single domain size calculated from the 111 peak (using Scherrer equation) depending on the number of domains. The black triangles represent CUB models (Table S 1); red diamonds - DEC models; yellow stars - ICO models.



## Supplementary Notes

Note S 1:

Density of gold:  $\rho_{Au} = 19.32 \text{ g/cm}^3$ ;

Volume of Au in 5% catalyst (1 mg):  $V_{Au} = \frac{0.001 * 0.05}{19.32} = 2.59 * 10^{-6} \text{ cm}^3$

If average NPs size  $\sim 5 \text{ nm}$ , the volume of one particle is:  $V_{Au NP} = \frac{4}{3} * \pi * r^3 = 5.24 * 10^{-19} \text{ cm}^3$

Therefore, the number of NPs in 1 milligram:  $N_{NP} = \frac{V_{Au}}{V_{Au NP}} = 4.94 * 10^{12}$

Note S 2:

The yellow stars in the lower right corner represent ICO models with 12431 and 14993 atoms. Using molecular dynamics simulation each model was equilibrated at 293 K for at least 30 psec. The ICO cluster consists of 20 domains. However, as it can be seen, the equation 1 gives wrong estimation of the number of domains. This is caused by a significant broadening of ICO 220 peak. The main reason for this broadening is an extraordinary strain distribution in a single ICO domain <sup>1</sup>.

One of the ICO models shown by yellow star (Fig. 3 (b)) consists of 14993 atoms. The single domain of this ICO consists of  $14993 / 20 = \sim 750$  atoms. From the Table S 1, one can roughly estimate the size of such domain (taking average of CUB models with 561 and 923 atoms). The size of single ICO domain will be  $\sim 2.6 \text{ nm}$ . Using Scherrer equation we can calculate the correct (220) FWHM (strain free) of such domain, which is equal to  $\sim 3.8$ . Once we consider the correct FWHM, the multidomain XRD approach points to the correct number of domains.

Another limitation of the MDXRD is caused by close distance between 111 - 200 and 220 - 311 peaks, resulting in overlap of peaks for very small clusters (smaller than 2.5 nm). This leads to a wrong estimation of 111 amplitude and 220 FWHM. Which also makes the multidomain XRD approach less precise for small clusters.

Note S 3:


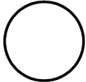
The analysis of **relaxed** computational models is especially important for the description of multidomain models similar to the model in Fig. 5, when it's difficult to visually estimate the average number of domains.

The analysis of  $H_{220}/H_{111}$  ratios as a function of 220 peak FWHMs for 10 **relaxed** gold DEC models is shown in the Figure S 5. The general equations are shown in equations 1 and 2. The updated variables for the **relaxed** models are given in the table below (next to the triangle). In addition, it must be taken into account that the  $H_{220}/H_{111}$  ratio is shape dependent (Figure S 7). This feature is less important for experimental powder samples because of the high number of different crystalline shapes. However, for computational simulations, when all you have is the only one model, then shape become important. Our experiment with the shape of a single domain cluster showed that for a spherical particle these variables are slightly different from those for the one domain DEC model.

$$\frac{H_{220}}{H_{111}} = \gamma * FWHM_{220} + [\alpha * \ln(Num.dom.) + \beta] \quad 1$$

$$Num.dom. = \exp\left(\frac{\beta + \gamma * FWHM - \frac{H_{220}}{H_{111}}}{-\alpha}\right) \quad 2$$

For relaxed computational models of gold particles, the parameters of equation 2 are equal:

Shape	$\alpha$	$\beta$	$\gamma$
One domain of DEC 	-0.057	0.438	-0.0145
One domain spherical model 	-0.054	0.425	-0.015

Note S 4:

For the analysis of all experimental data, the following parameters were used:

$$\alpha = - 0.06$$

$$\gamma = - 0.0065$$

Since the  $H_{(220)}/H_{(111)}$  ratio is individual for each element, the  $\beta$  parameter is dependent on the material and the energy of the X-ray beam (the following data are given for the Cu radiation):

- for pure Au:  $\beta = 0.32$  (according to the JCPDS no. 04-0784 )

- for pure Pt:  $\beta = 0.31$  (according to the JCPDS no. 04-0802 )

- for pure Ag:  $\beta = 0.25$  (according to the JCPDS no. 04-0783 )

- for pure Cu:  $\beta = 0.21$  (according to the JCPDS no. 85-1326 )

AgPt@PVP@SiO<sub>2</sub>:

The ratio of Ag to Pt is 55 to 45, the resulting  $\beta$  parameter will be equal to the weighted mean of the two pure constituents:

- for Ag<sub>55</sub>Pt<sub>45</sub>:  $\beta = 0.25*0.55 + 0.31*0.45 = 0.28$

CuAg@PVP@SiO<sub>2</sub>:

Since the ratio of Cu to Ag is 52 to 48, the resulting  $\beta$  parameter will be equal:

- for Cu<sub>52</sub>Ag<sub>48</sub>:  $\beta = 0.21*0.52 + 0.25*0.48 = 0.23$

Supplementary Table

List of CUB models

Number of atoms	Shells	Size, [nm]
147	3	1.46
309	4	1.87
561	5	2.40
923	6	2.81
1415	7	3.35
2057	8	3.76
2869	9	4.30
3871	10	4.71
5083	11	5.13
6525	12	5.66
8217	13	6.21
10179	14	6.61
12431	15	7.17
14993	16	7.56
17885	17	8.12
21127	18	8.51

List of DEC models

Number of atoms			m=n	p	Relaxed size, [nm]
Total	1 domain	Central row			
1228	243	13	5	3	3.15
1840	365	15	6	3	3.62
2622	521	17	7	3	4.13
3594	715	19	8	3	4.62
4776	951	21	9	3	5.10
6188	1233	23	10	3	5.52
7850	1565	25	11	3	6.06
9782	1951	27	12	3	6.54
12004	2395	29	13	3	7.02
14536	2901	31	14	3	7.50
17398	3473	33	15	3	7.98
20610	4115	35	16	3	8.44
24192	4831	37	17	3	8.95

Table S 1 List of all used CUB and DEC models. Parameters “m, n, p” describe the shape of the Marks DEC model <sup>2</sup>. After calculating the volume of the model, assuming a spherical shape of the cluster, the diameter was calculated.

Group	Sample ID	XRD			MDXRD				TEM		SAXS		
		W-H plot Size, [nm]	Scherrer equation		$H_{(220)}/$ $H_{(111)}$	220 FWHM	Num. Dom.	Mean size, [nm]	Num. Dom.	Mean size, [nm]	Num. Dom.	Mean size, [nm]	
			111 peak Size, [nm]	220 peak Size, [nm]									
Main samples	1	Au@PVP 1	2.34	2.08	1.51	0.19	6.53	4.07	2.18	4.40	2.25	6.37	2.62
		Au@PVP 2	3.74	2.34	1.55	0.17	6.34	5.38	2.57	5.81	2.66	7.04	3.01
		Au@PVP 3	3.46	2.40	1.60	0.17	6.15	6.13	2.87	6.15	2.87	6.59	3.07
	2	Au@PVP@SiO <sub>2</sub> RT	3.83	5.70	3.72	0.21	2.64	4.46	7.09	4.01	6.71	4.33	6.98
		Au@PVP@SiO <sub>2</sub> 400°C	4.99	6.61	3.72	2.96	2.64	2.96	5.83	3.56	6.34	3.98	6.70
		Au@PVP@SiO <sub>2</sub> 500°C	5.50	6.68	4.29	3.08	2.29	3.08	6.94	2.58	6.44	2.61	6.47
		Au@PVP@SiO <sub>2</sub> 600°C	5.40	6.95	4.36	2.92	2.25	2.92	6.91	2.75	6.74	2.72	6.71
		Au@PVP@SiO <sub>2</sub> 800°C	5.05	3.93	2.64	0.20	3.76	5.58	5.33	5.73	5.41	2.14	7.97
	3	Au <sub>55</sub> Pt <sub>45</sub> @SiO <sub>2</sub> RT	1.66	2.85	2.09	0.19	4.73	5.50	3.92	6.29	4.21	4.34	3.48
		Au <sub>55</sub> Pt <sub>45</sub> @SiO <sub>2</sub> 450°C	5.05	3.93	2.64	0.19	3.76	5.58	5.33	5.73	5.41	4.88	4.96
4	Au@C	1.66	2.85	2.09	0.18	4.73	5.50	3.92	6.29	4.21	4.17	3.99	
Supplement samples	5	Ag <sub>44</sub> Pt <sub>56</sub> @SiO <sub>2</sub> RT	1.66	2.29	1.89	0.12	5.22	8.30	3.78	6.11	3.64		
		Ag <sub>44</sub> Pt <sub>56</sub> @SiO <sub>2</sub> 400°C	3.61	3.16	2.80	0.21	2.80	2.50	3.67	1.61	3.42		-
		Ag <sub>44</sub> Pt <sub>56</sub> @SiO <sub>2</sub> 600°C	6.87	6.10	6.52	0.23	6.52	2.20	8.94	3.20	11.14		
	6	Cu <sub>52</sub> Ag <sub>48</sub> @SiO <sub>2</sub> RT	1.82	2.82	3.02	0.16	3.25	2.39	3.97	3.09	4.68		
		Cu <sub>52</sub> Ag <sub>48</sub> @SiO <sub>2</sub> 400°C	6.77	7.38	6.40	0.17	1.53	2.31	8.95	2.56	9.89		-
		Cu <sub>52</sub> Ag <sub>48</sub> @SiO <sub>2</sub> 600°C	142.76	43.45	27.24	0.15	0.36	3.87	50.17	12.78	121.20		

Table S 2 List of experimental samples characterized by XRD (Williamson-Hall analysis – W-H), MDXRD, TEM and SAXS; Num.Dom. – number of domains.

## Supplementary Methods

### Method S 1 Au@PVP 1:

2 g of PVP K 30 (40 kDa, Carl Roth, Germany) was dissolved in 20 ml of milli-Q water (Milli-Q Advantage system from Merck), then poured into a dialysis bag, with a cut-off size of 100–500 g.mol<sup>-1</sup> (spectra/Por® Biotech, US). The dialysis bag was then immersed in milli-Q water and left to equilibrate under moderate magnetic stirring for 8 days. The water was exchanged 11 times.

7.17 ml of dialyzed PVP solution was diluted by 12.4 ml of water. After that the 9.25 ml of 25.4 mM H<sub>2</sub>AuCl<sub>4</sub> \* 3 H<sub>2</sub>O (99.9%, Alfa Aesar), was mixed with PVP solution and mixed under moderate magnetic stirring for 30 min in an ice bath.

Another 7.17 ml of dialyzed PVP solution was diluted by 22.8 ml water and placed in an ice bath for 30 min. Then, 5 min before the reduction reaction 40 mg of NaBH<sub>4</sub> (99%, Sigma-Aldrich) was added and mixed.

Ice cooled NaBH<sub>4</sub> solution was quickly injected into the solution with the gold precursor. To remove Na<sup>+</sup> and Cl<sup>-</sup> ions the obtained mixture was subsequently dialyzed in milli-Q water (buffer to sample ratio was 100:1): the first buffer change after 2-3 hours, the second one after 4-5 hours, the third one after ~24 hours.

The sample was dried at <30°C and at pressure <90 k Pa.

In order to improve the analysis of XRD peaks positions, an aliquot of a polycrystalline quartz was added to the sample.

### Method S 2 Au@PVP@SiO<sub>2</sub> RT:

0.717 g of PVP K 30 (40 kDa, Carl Roth, Germany) was dissolved in 21.6 ml of Demi water and mixed with 9.25 ml of 25.4 mM H<sub>2</sub>AuCl<sub>4</sub>\*3 H<sub>2</sub>O (99.9%, Alfa Aesar), then stirred for 30 min in an ice bath.

The next step is a preparation of the reduction agent: 0.717 g of PVP K 30 was dissolved in 32 ml of Demi water and stirred for 30 min in an ice bath. Then, 5 min before the reduction reaction 55 mg of NaBH<sub>4</sub> (99%, Sigma-Aldrich) were added and mixed. After that, the ice cooled NaBH<sub>4</sub> solution was quickly injected into the solution with the gold precursor.

The preparation of SiO<sub>2</sub> spheres consisted of few steps. The first one, was mixing of NPs solution with 6.88 ml of NH<sub>4</sub>OH (reagent grade, 25%, Chempur) and 100 ml of 2-propanol (99.7%, p.p.a.

basic, POCH Basic). The second step was to dissolve of 3.72 ml TEOS (reagent grade, 98%, Sigma-Aldrich) in 87.72 ml of 2-propanol. The final step was to mix both solutions and vigorously stir for 2h to ensure complete polymerization of silica. Then, the catalyst was filtered.

After all, the sample was dried at  $<30^{\circ}\text{C}$  at pressure  $<90$  k Pa.

### **Method S 3 AuPt@SiO<sub>2</sub> RT:**

To prepare initial Au-Pt NPs, 548 ml of 0.484 mM  $\text{HAuCl}_4 \cdot 3 \text{H}_2\text{O}$  (99.9%, Alfa Aesar) was mixed with 548 ml of 0.396 mM  $\text{H}_2\text{PtCl}_6 \cdot 6\text{H}_2\text{O}$  (99.9%, Alfa Aesar) and intensively stirred for at least 5 min at room temperature. Then, 2200 ml of 22 mM PVP aqueous solution (monomer units) was added to the AuPt solution and mixed for at least 30 min in an ice water bath at  $\sim 0^{\circ}\text{C}$ .

To reduce the catalyst, 363 ml of 33 mM  $\text{NaBH}_4$  ice-cold aqueous solution was slowly added to the AuPt solution and vigorously stirred for 1 hour. The product was dried in rotor evaporator.

Preparation of  $\text{SiO}_2$  amorphous matrix consisted of few steps. In the first one, the colloid NPs solution was mixed with 8.16 ml of  $\text{NH}_4\text{OH}$  (reagent grade, 25%, Chempur) and 234 ml of 2-propanol (99.7%, p.p.a. basic, POCH Basic). The second step was to dissolve of 4.34 ml TEOS (reagent grade, 98%, Sigma-Aldrich) in 104 ml of 2-propanol and 1742 ml of  $\text{H}_2\text{O}$ . The final step was to mix both solutions and vigorously stir for 2h to ensure complete polymerization of silica. The product was dried in rotor evaporator.

Then 210 ml of 2-propanol was added to the NPs mixture. The obtained solution was filtered and rinsed with 2-propanol. After all, the sample was dried overnight at  $60^{\circ}\text{C}$  at pressure  $<80$  k Pa.

According to the XRF, the Au and Pt contents were 55% and 45%, respectively.

### **Method S 4 Au@C:**

The Au@C nanoparticles were synthesized based on J. Turkevich method<sup>3</sup> and modified K. C. Grabar<sup>4</sup> methods.

400 mg of Vulcan XC 72 (Cabot Corporation) was suspended under ultrasonication in 85 ml mixture of propan-2-ol (ppa, Stanlab) and distilled  $\text{H}_2\text{O}$  (volume ratio 3:1).

To prepare the gold precursor solution: 20 ml of  $\text{HAuCl}_4 \cdot 3 \text{H}_2\text{O}$  (0.0254 M, 99.9%, Alfa Aesar) was diluted under stirring at 293 K with 1725 ml of distilled  $\text{H}_2\text{O}$  and then 17 ml of 4%<sub>wt.</sub>  $\text{Na}_3\text{C}_6\text{H}_5\text{O}_7$  (ppa, Chempur) solution was added.

To prepare a reducing agent solution: 15 mg of  $\text{NaBH}_4$ , (99%, Sigma-Aldrich) was dissolved in 17 ml of 4%<sub>w.t.</sub> aqueous  $\text{Na}_2\text{C}_2\text{O}_4$  solution.

Five minutes after the start of the reduction reaction, a suspension of Vulcan XC 72 was added to the solution of nanoparticles. The mixture was stirred for 48 h in darkness. After that, it was filtered and washed with water to remove chloride and sodium ions. Finally, the catalyst was dried under vacuum at  $<40^\circ\text{C}$ .

#### **Method S 5 AgPt@PVP@SiO<sub>2</sub>:**

To synthesis the AgPt NPs we used exactly the method which was described at **Method S 3**, with the same molar ratio of components. The only difference was in used precursors: we used  $\text{H}_2\text{PtCl}_6 \cdot 6\text{H}_2\text{O}$  (99.9%, Alfa Aesar,) and  $\text{AgNO}_3$  (99.9%, POCH, Poland). According to the XRF, the Ag and Pt contents were 44% and 56%, respectively.

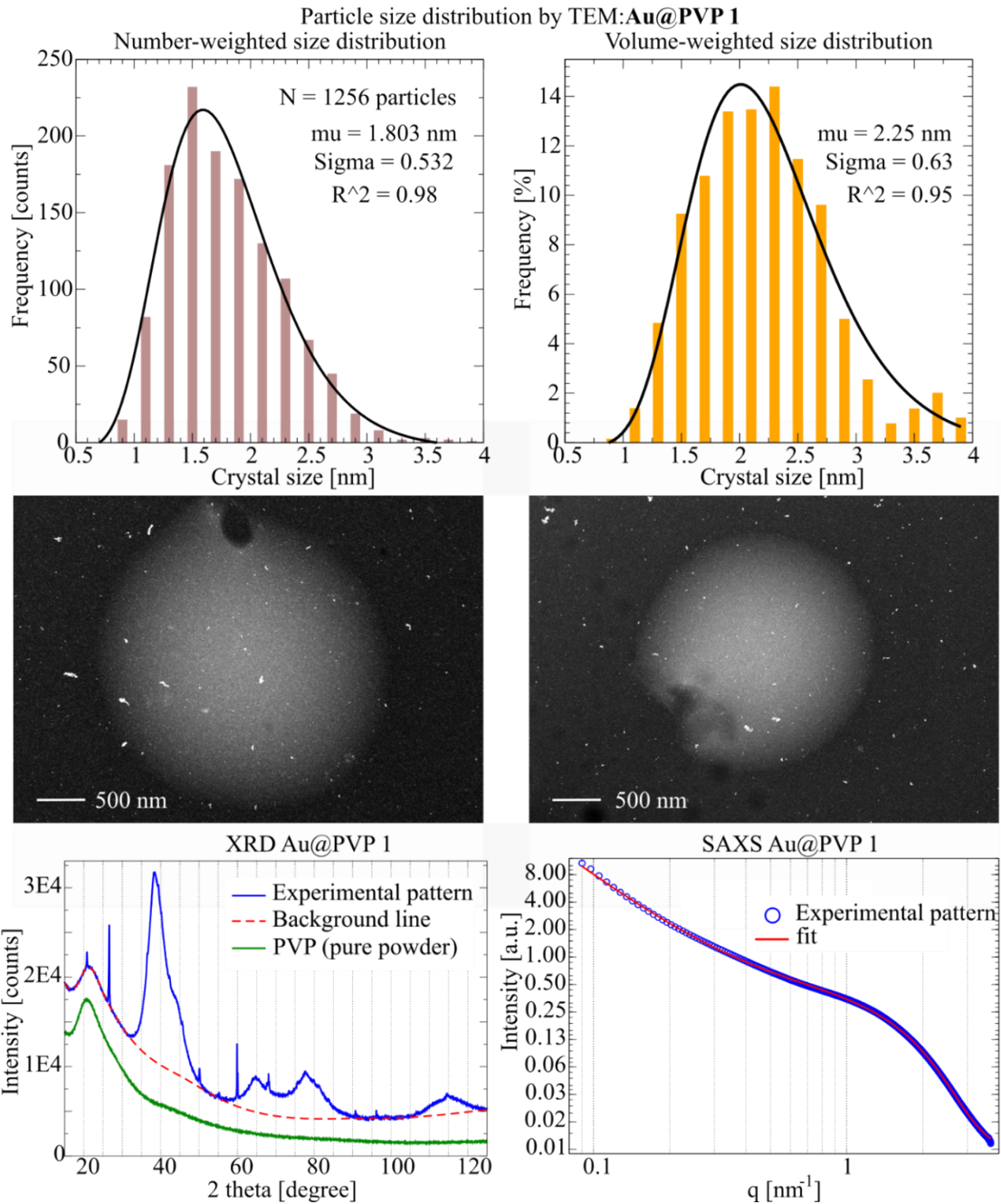
#### **Method S 6 CuAg@PVP@SiO<sub>2</sub>:**

To synthesis the CuAg NPs we used exactly the method which was described at **Method S 3**, with the same molar ratio of components. The only difference was the used precursors: We used  $\text{Cu}(\text{NO}_3)_2 \cdot 3\text{H}_2\text{O}$  (99.9%, Chempur, Piekary Śląskie, Poland) and  $\text{AgNO}_3$  (99.9%, POCH, Poland). According to the XRF, the Cu and Pt contents were 52% and 48%, respectively.

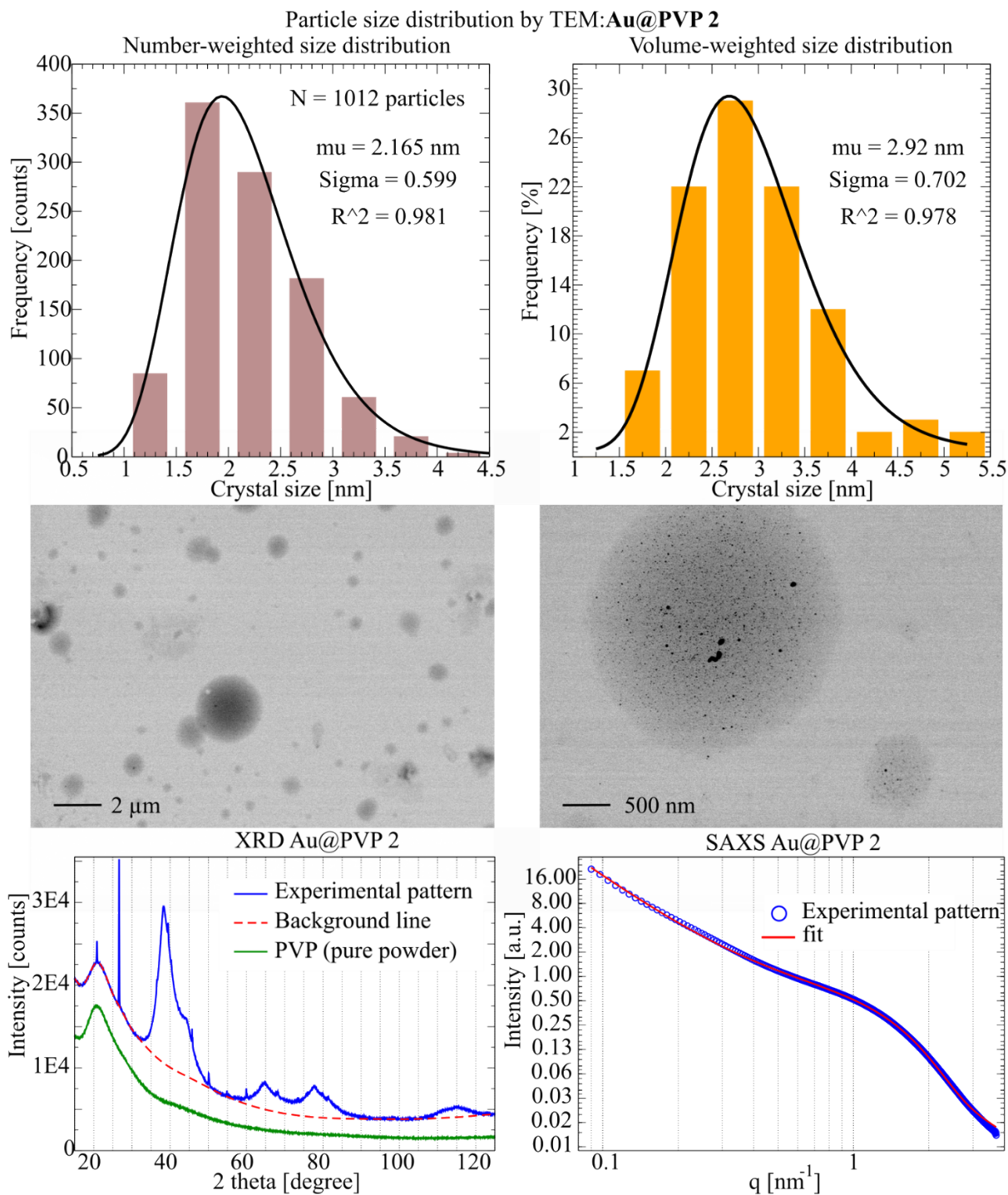


## Supplementary Data

### GROUP 1 Au@PVP

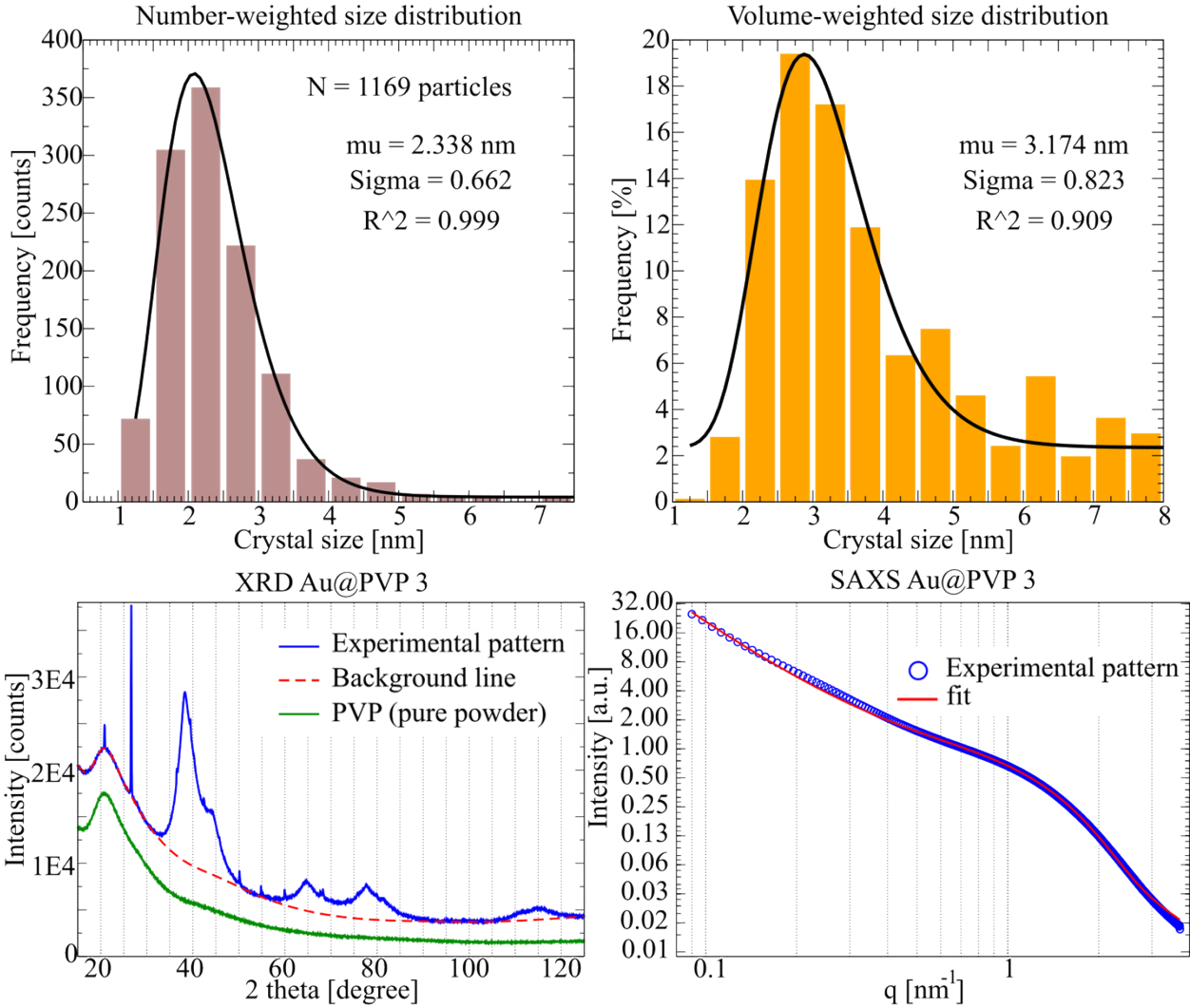


Data S 1 Au@PVP 1 sample analysis: TEM GSD; XRD pattern of the experimental sample (blue line), applied background (red dotted line), and scaled diffraction pattern of the supporting material (green line). The narrow diffraction peaks shown in the XRD pattern correspond to polycrystalline quartz, which was used as a reference for peak position calibration. PVP did not form any regular structures, so it does not affect the SAXS pattern (see Data S 2).



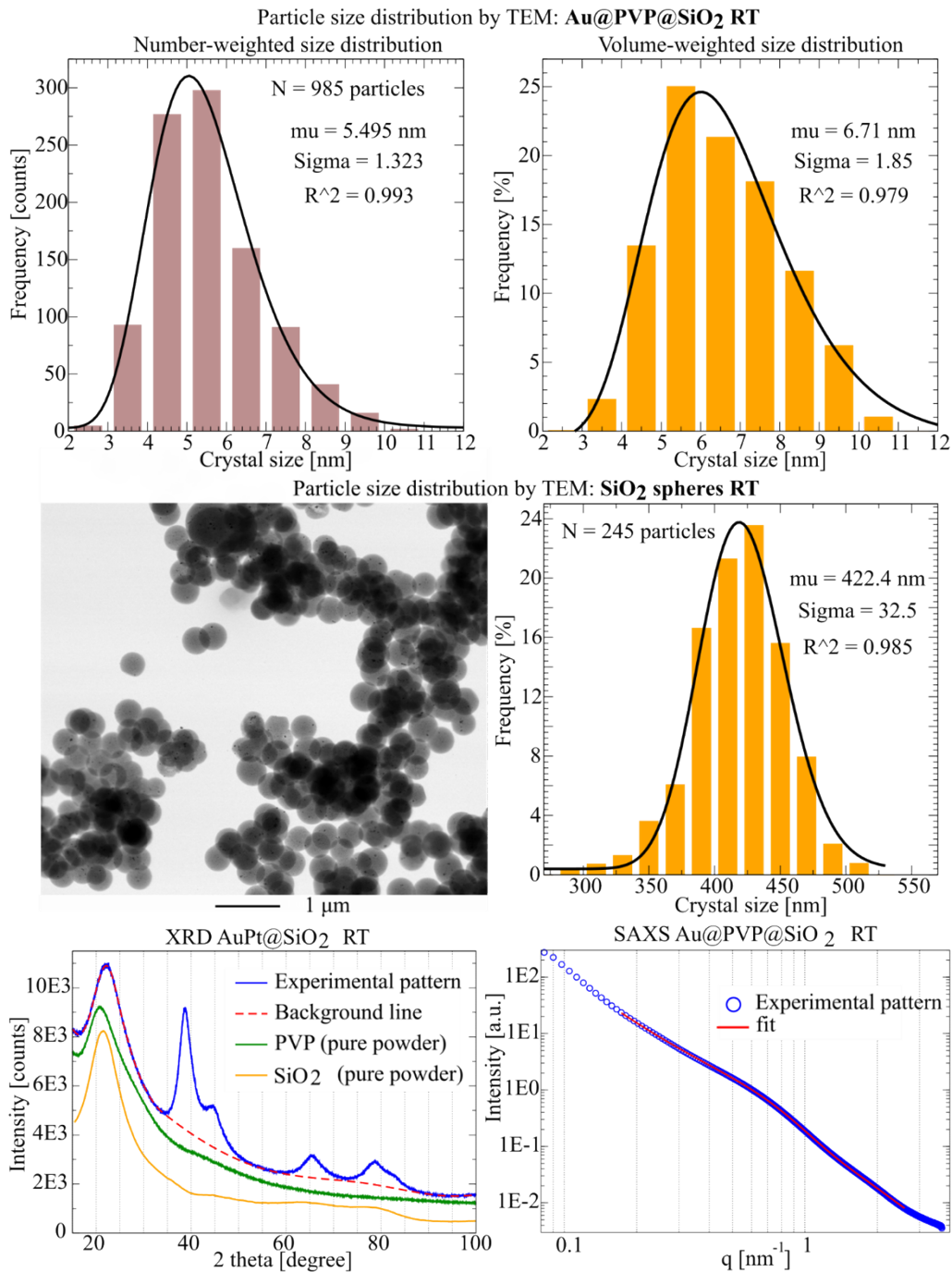
Data S 2 Au@PVP 2 sample analysis: TEM GSD; XRD pattern of the experimental sample (blue line), applied background (red dotted line), and scaled diffraction pattern of the supporting material (green line). The narrow diffraction peaks shown in the XRD spectra correspond to polycrystalline quartz, which was used as a reference for peak position calibration. PVP did not form any regular structures, so it does not affect the SAXS pattern.

Particle size distribution by TEM: **Au@PVP 3**



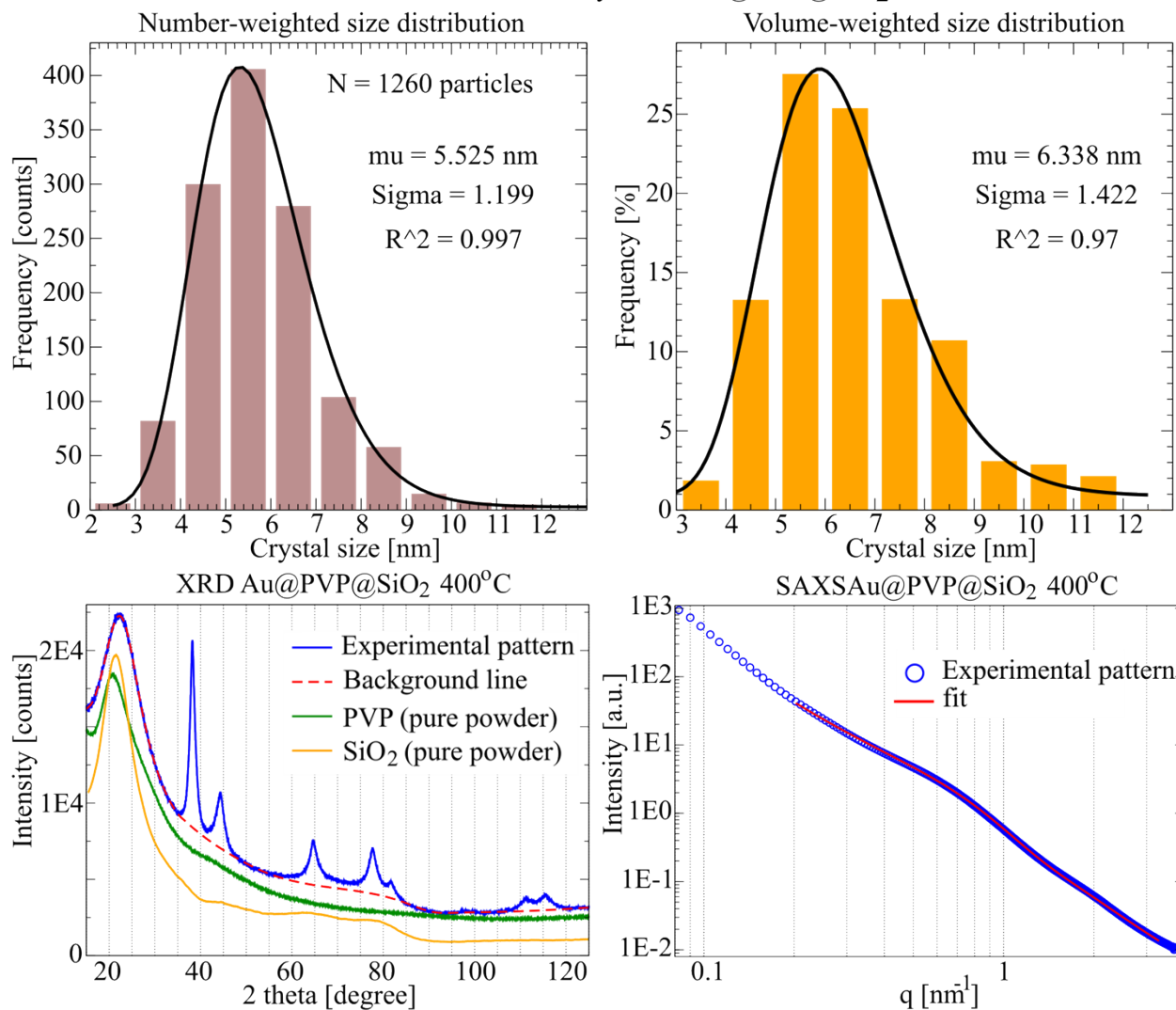
Data S 3 Au@PVP 3 sample analysis: TEM GSD; X-ray diffraction pattern of the experimental sample (blue line), applied background (red dotted line), and scaled diffraction pattern of the supporting material (green line). The narrow diffraction peaks shown in the XRD spectra correspond to polycrystalline quartz, which was used as a reference for peak position calibration. PVP did not form any regular structures, so it does not affect the SAXS pattern

## GROUP 2 Au@SiO<sub>2</sub>



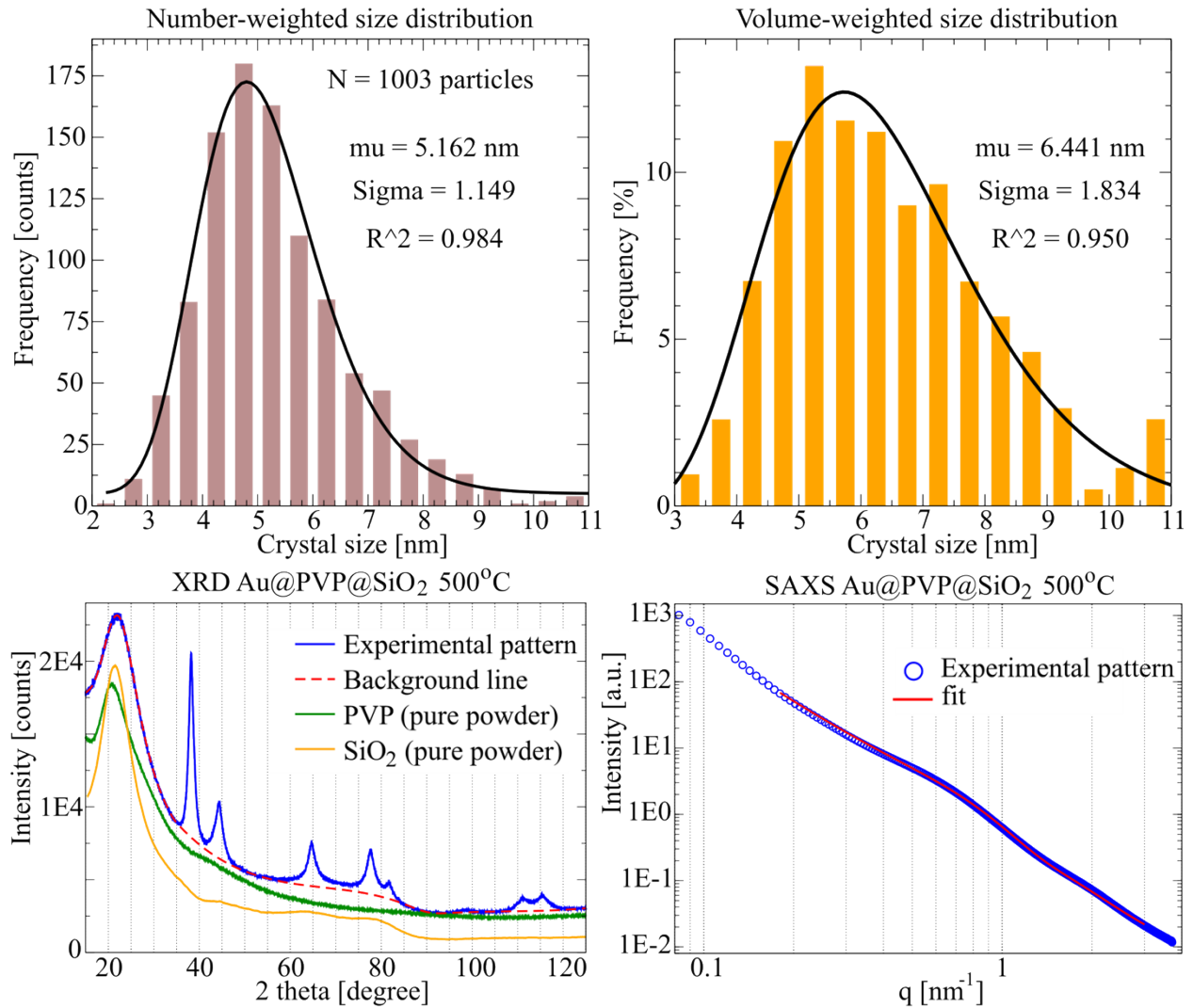
Data S 4 Au@PVP@SiO<sub>2</sub> RT sample analysis: TEM GSD; XRD pattern of the experimental sample (blue line), applied background (red dotted line), and scaled diffraction pattern of the supporting material (yellow and green lines). Au NPs were encapsulated in SiO<sub>2</sub> spheres with an average radius of  $\sim 420$  nm. Therefore, SAXS fitting range starts with a  $q$  value of  $0.17 \text{ nm}^{-1}$ .

Particle size distribution by TEM: **Au@PVP@SiO<sub>2</sub> 400°C**



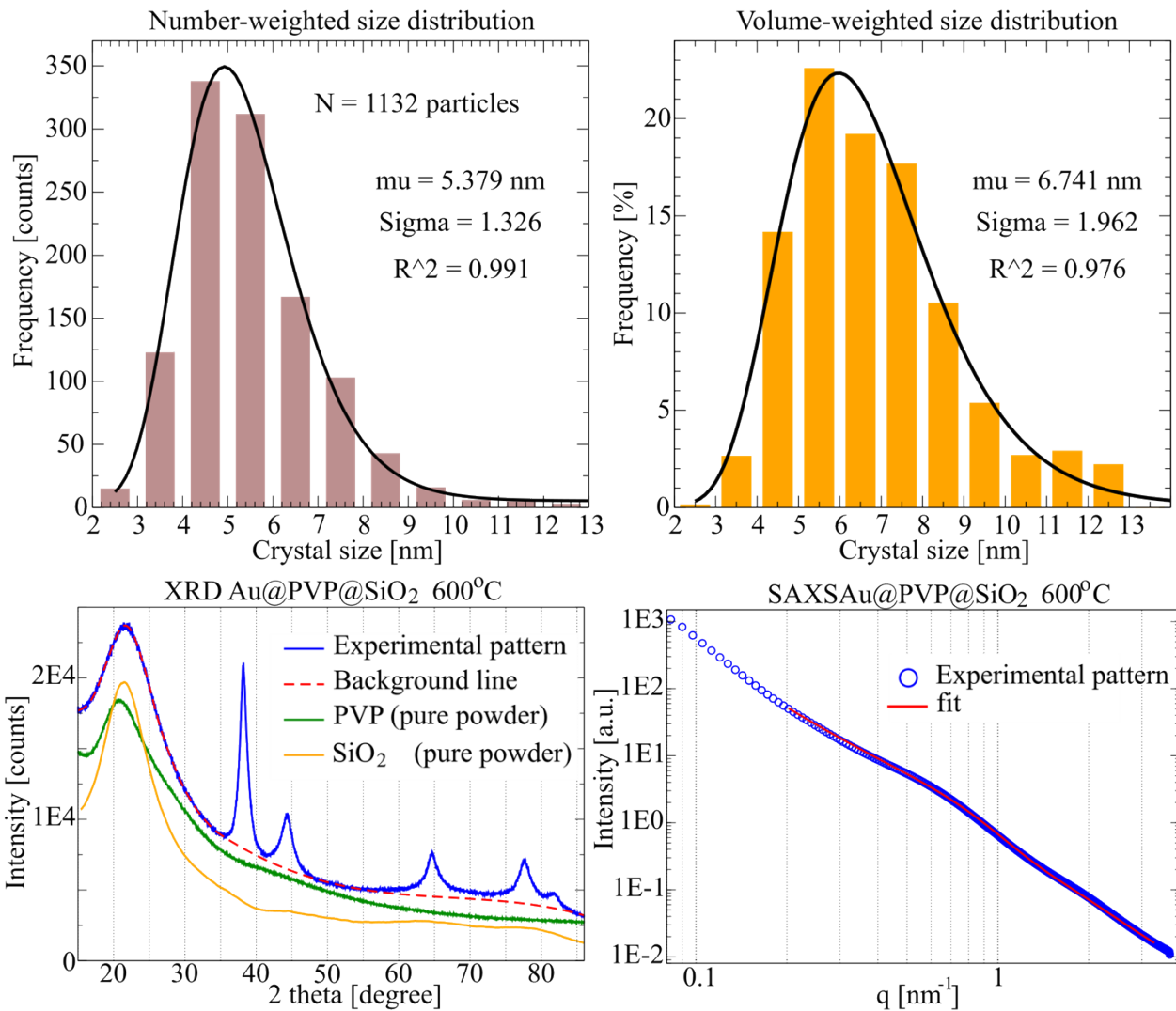
Data S 5 Au@PVP@SiO<sub>2</sub> 400 °C sample analysis: TEM GSD; X-ray diffraction pattern of the experimental sample (blue line), applied background (red dotted line), and scaled diffraction pattern of the supporting material (yellow and green lines). Au NPs were encapsulated in SiO<sub>2</sub> spheres with a regular size distribution. Therefore, SAXS fitting range starts with a q value of 0.2 nm<sup>-1</sup>.

Particle size distribution by TEM: Au@PVP@SiO<sub>2</sub> 500<sup>o</sup> C



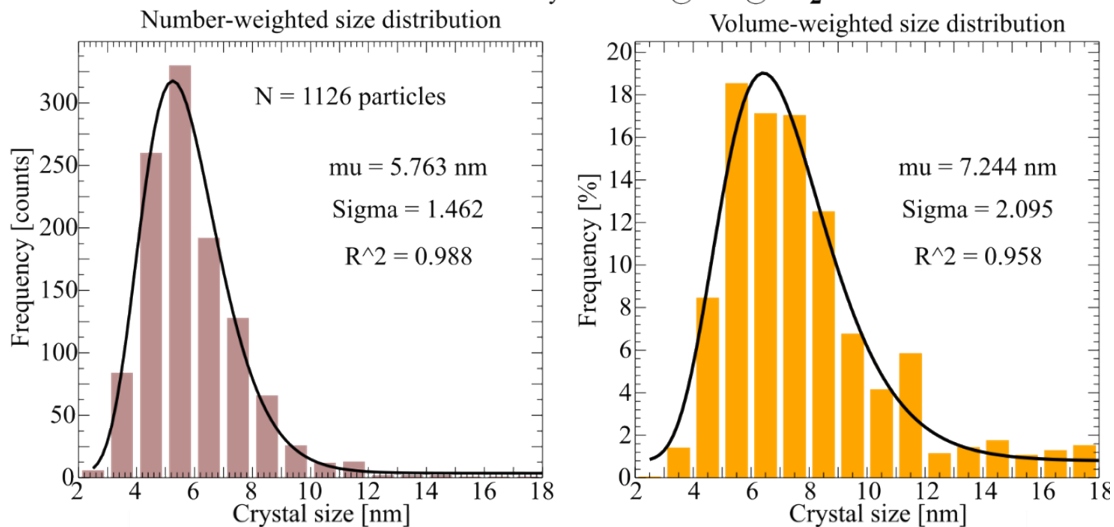
Data S 6 Au@PVP@SiO<sub>2</sub> 500 °C sample analysis: TEM GSD; X-ray diffraction pattern of the experimental sample (blue line), applied background (red dotted line), and scaled diffraction pattern of the supporting material (yellow and green lines). Au NPs were encapsulated in SiO<sub>2</sub> spheres with a regular size distribution. Therefore, SAXS fitting range starts with a q value of 0.18 nm<sup>-1</sup>.

Particle size distribution by TEM: **Au@PVP@SiO<sub>2</sub> 600<sup>o</sup> C**

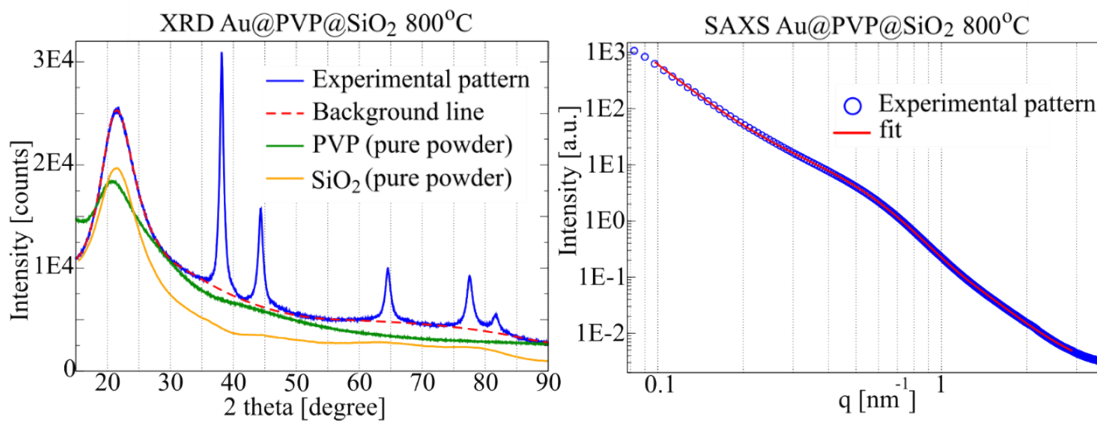
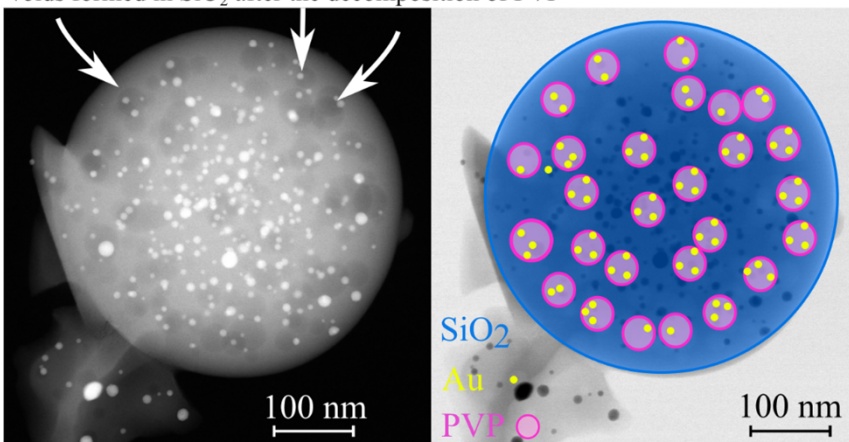


Data S 7 Au@PVP@SiO<sub>2</sub> 600 °C sample analysis: TEM GSD; X-ray diffraction pattern of the experimental sample (blue line), applied background (red dotted line), and scaled diffraction pattern of the supporting material (yellow and green lines). Au NPs were encapsulated in SiO<sub>2</sub> spheres with an average radius of ~420 nm. Therefore, SAXS fitting range starts with a q value of 0.2 nm<sup>-1</sup>.

Particle size distribution by TEM: Au@PVP@SiO<sub>2</sub> 800<sup>o</sup> C



Voids formed in SiO<sub>2</sub> after the decomposition of PVP

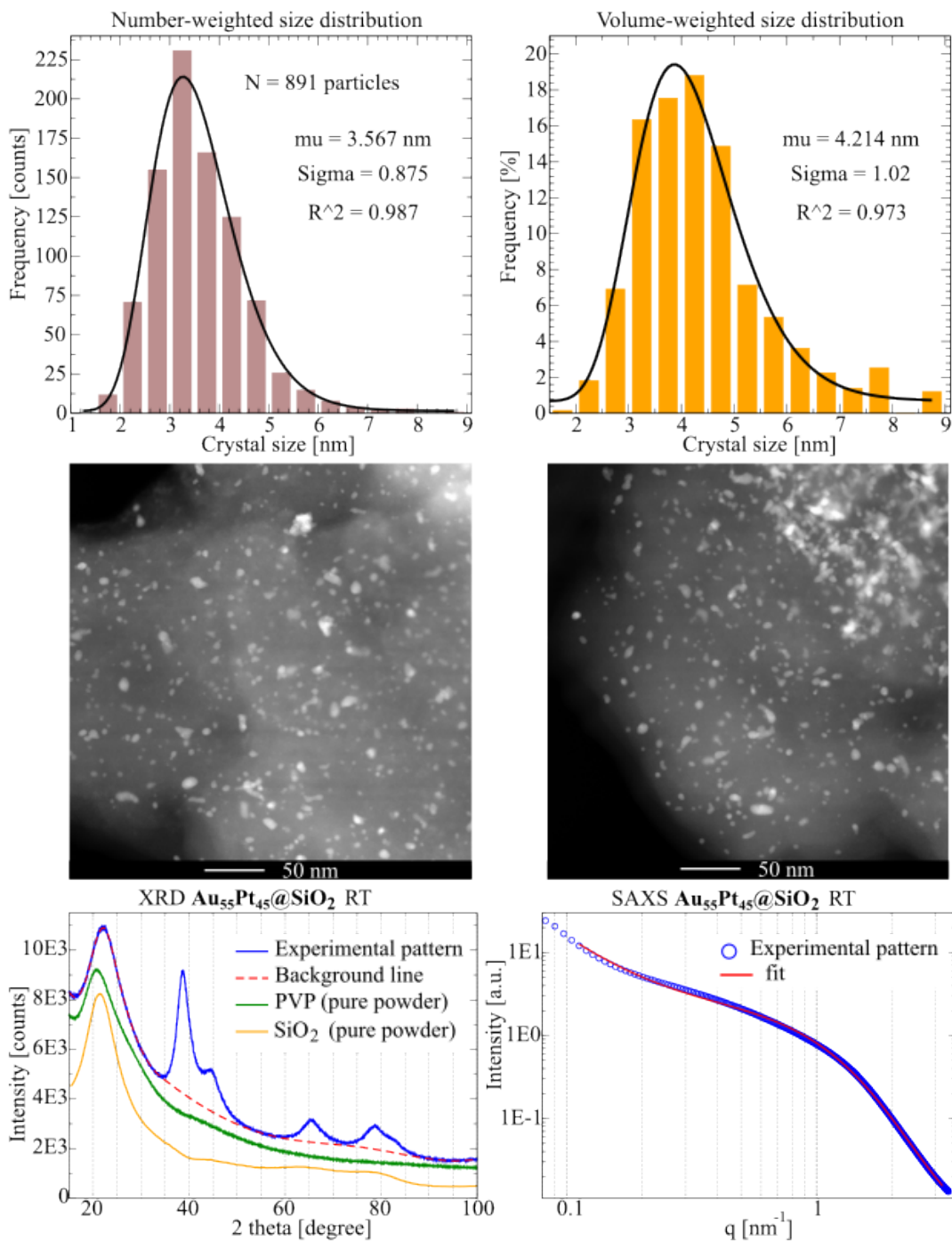


Data S 8 Au@PVP@SiO<sub>2</sub> 800 °C sample analysis: TEM GSD; X-ray diffraction pattern of the experimental sample (blue line), applied background (red dotted line), and scaled diffraction pattern of the supporting material (yellow and green lines). SiO<sub>2</sub> spheres were destroyed therefore SAXS fitting range starts with a q value of 0.1 nm<sup>-1</sup>.



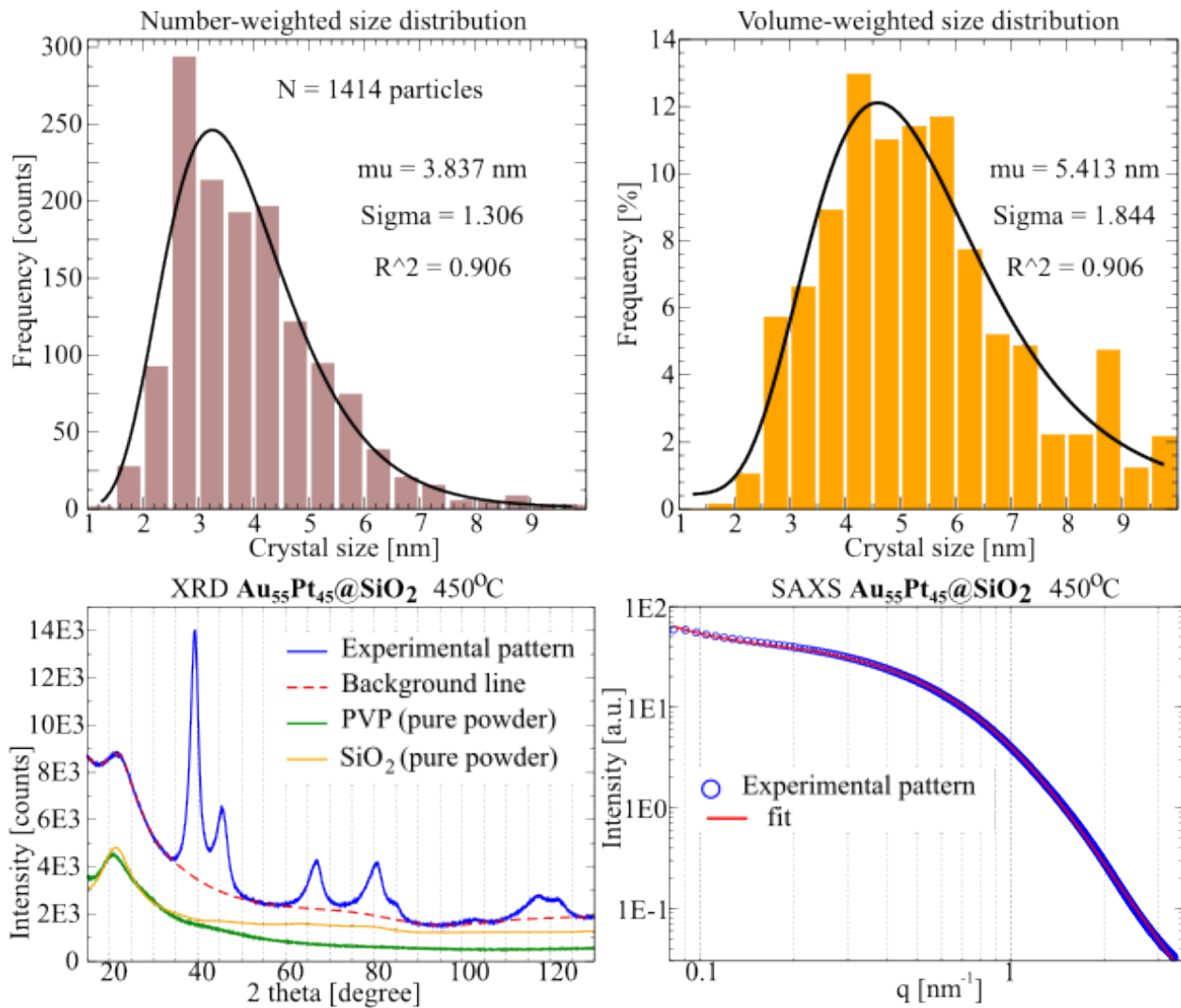
GROUP 3 AuPt@SiO<sub>2</sub>

Particle size distribution by TEM: Au<sub>55</sub>Pt<sub>45</sub>@SiO<sub>2</sub> RT



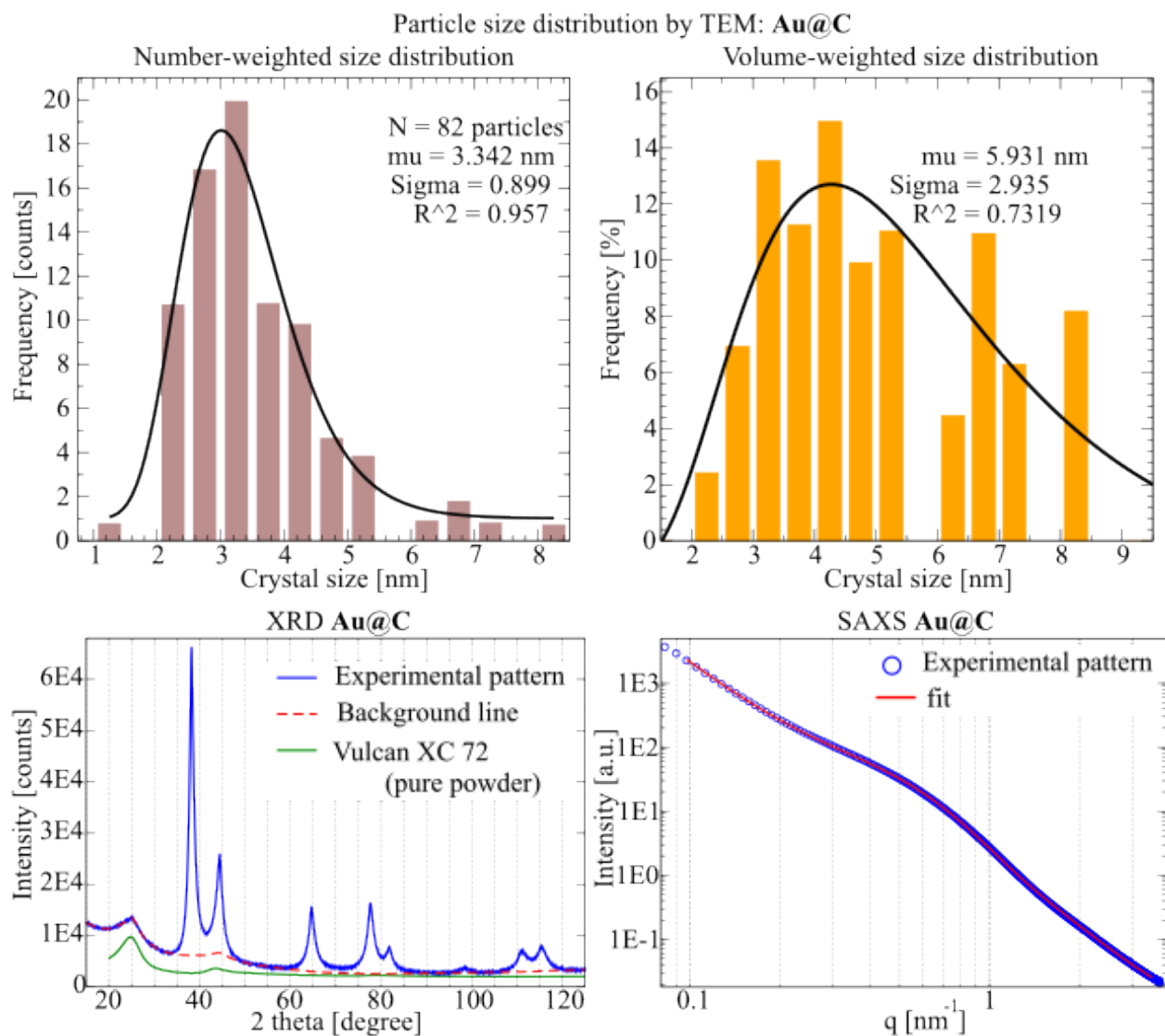
Data S 9 Au<sub>55</sub>Pt<sub>45</sub>@PVP@SiO<sub>2</sub> RT sample analysis: TEM GSD; X-ray diffraction pattern of the experimental sample (blue line), applied background (red dotted line), and scaled diffraction pattern of the supporting material (yellow and green lines). According to the TEM EDX mapping analysis, all NPs were in the form of an alloy.

Particle size distribution by TEM: **Au<sub>55</sub>Pt<sub>45</sub>@SiO<sub>2</sub> 450°C**



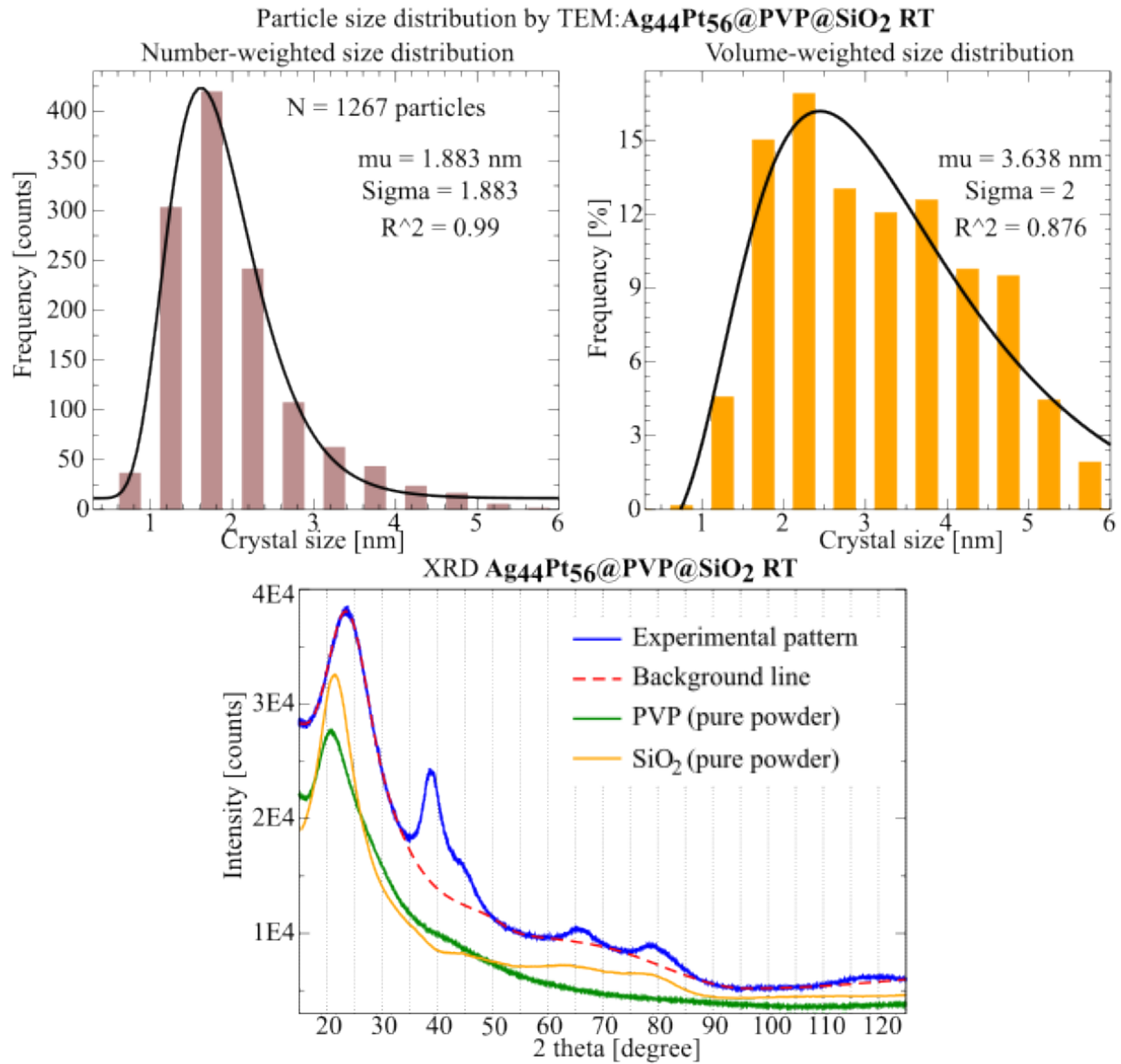
Data S 10 AuPt@PVP@SiO<sub>2</sub> 450 °C sample analysis: TEM GSD; X-ray diffraction pattern of the experimental sample (blue line), applied background (red dotted line), and scaled diffraction pattern of the supporting material (yellow and green lines). According to the TEM EDX mapping analysis, all NPs were in core-shell and alloy forms.

## GROUP 4 Au@C

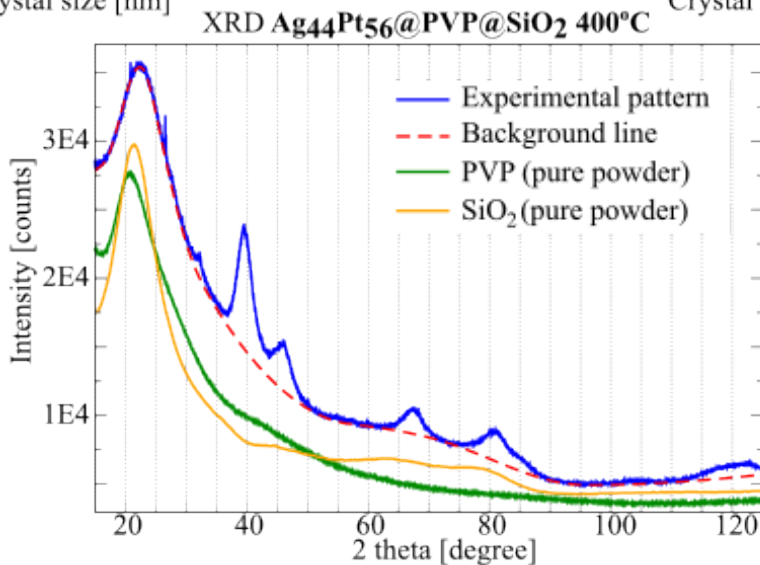
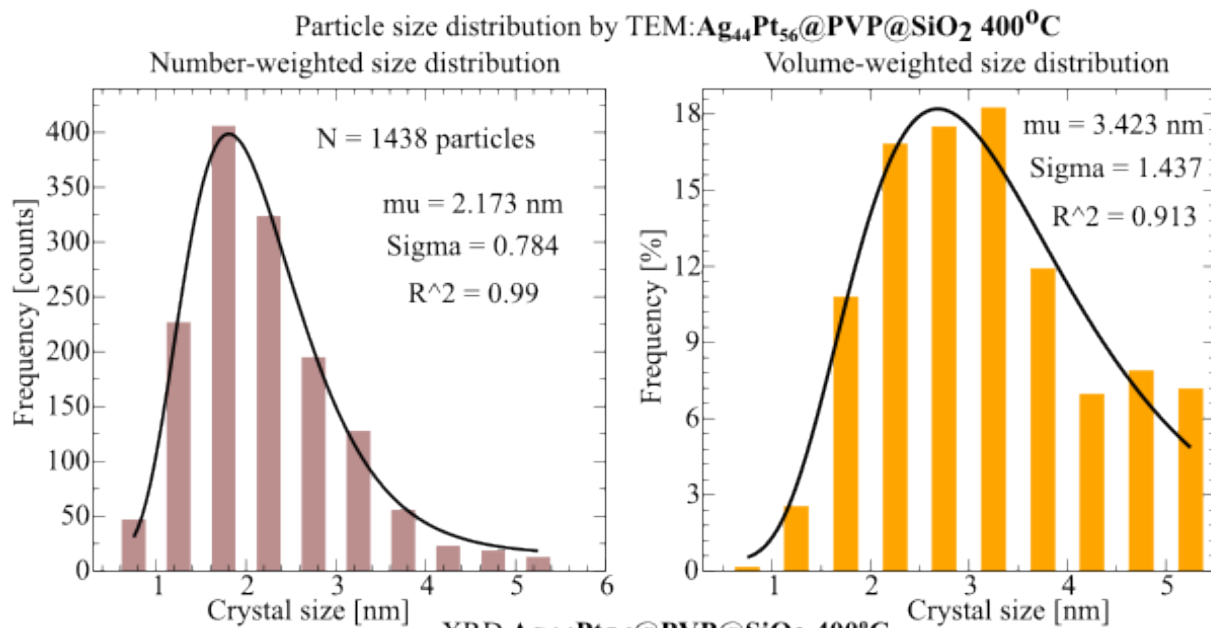


Data S 11 Au@C RT sample analysis: TEM GSD; X-ray diffraction pattern of the experimental sample (blue line), applied background (red dotted line), and scaled diffraction pattern of the supporting material (green line).

GROUP 5 AgPt@SiO<sub>2</sub>

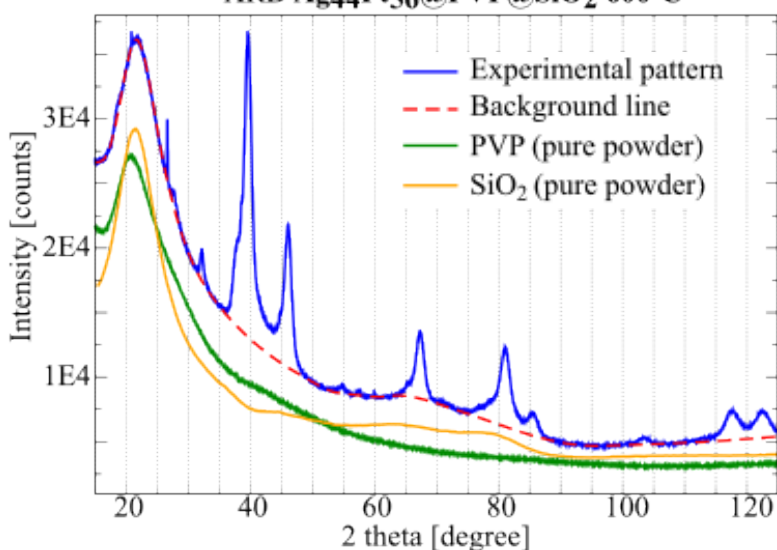
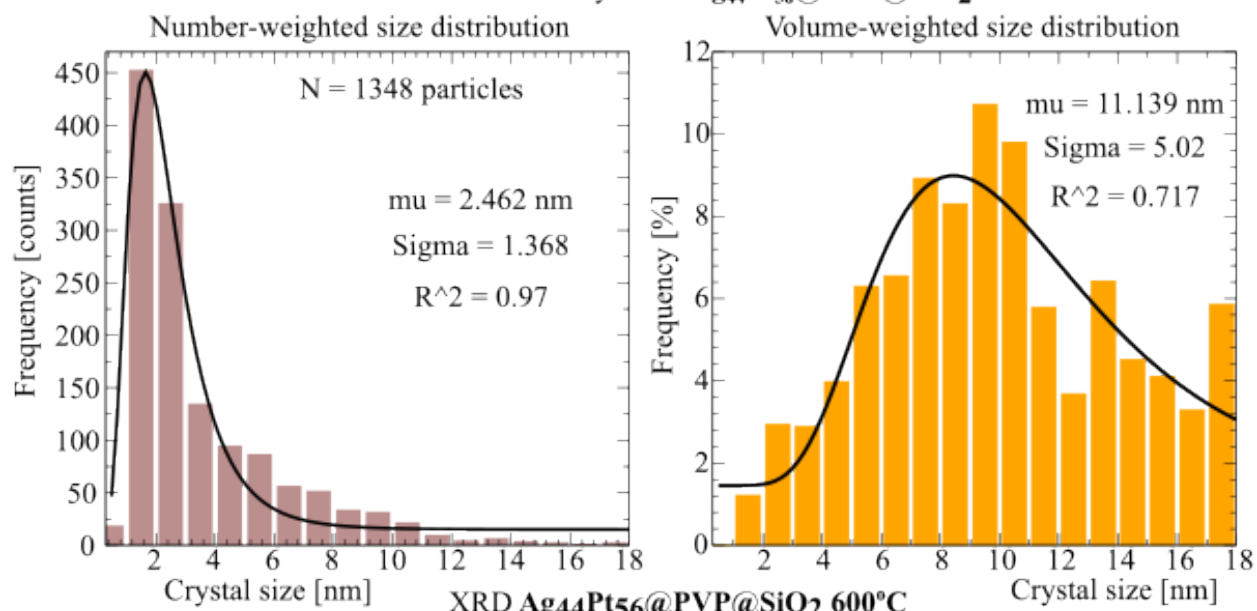


Data S 12 Ag<sub>44</sub>Pt<sub>56</sub>@PVP@SiO<sub>2</sub> RT sample analysis: TEM GSD; X-ray diffraction pattern of the experimental sample (blue line), applied background (red dotted line), and scaled diffraction pattern of the supporting material (yellow and green lines). According to the TEM EDX mapping analysis, NPs were found in three different states, in form of an alloy, as well as in the form of individual Ag and Pt nanoparticles.



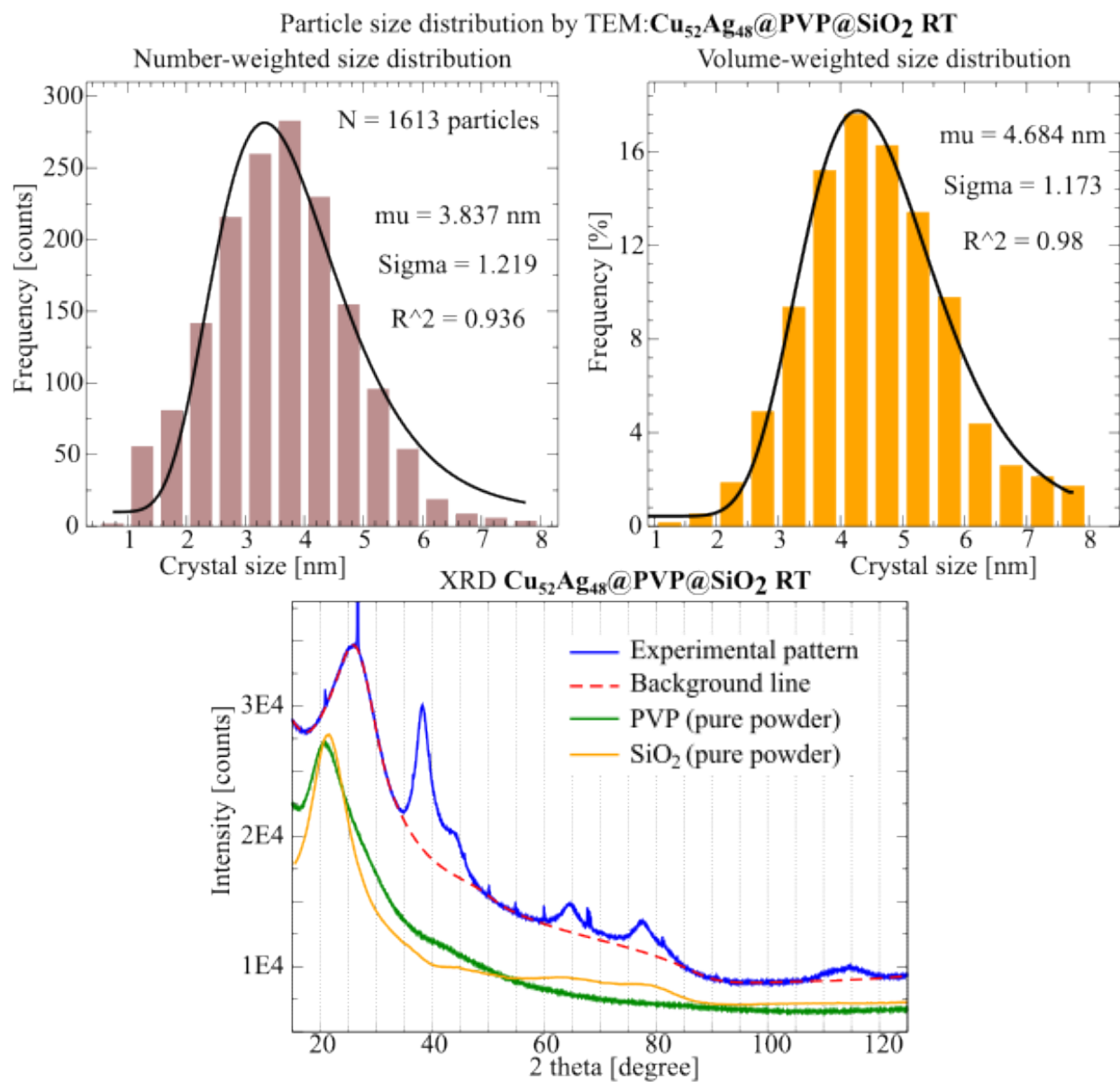
Data S 13  $\text{Ag}_{44}\text{Pt}_{56}@PVP@SiO_2$  400 °C sample analysis: TEM GSD; X-ray diffraction pattern of the experimental sample (blue line), applied background (red dotted line), and scaled diffraction pattern of the supporting material (yellow and green lines). According to the TEM EDX mapping analysis, NPs were found in three different states, in form of an alloy, as well as in the form of individual Ag and Pt nanoparticles.

Particle size distribution by TEM:  $\text{Ag}_{44}\text{Pt}_{56}@PVP@SiO_2$  600°C

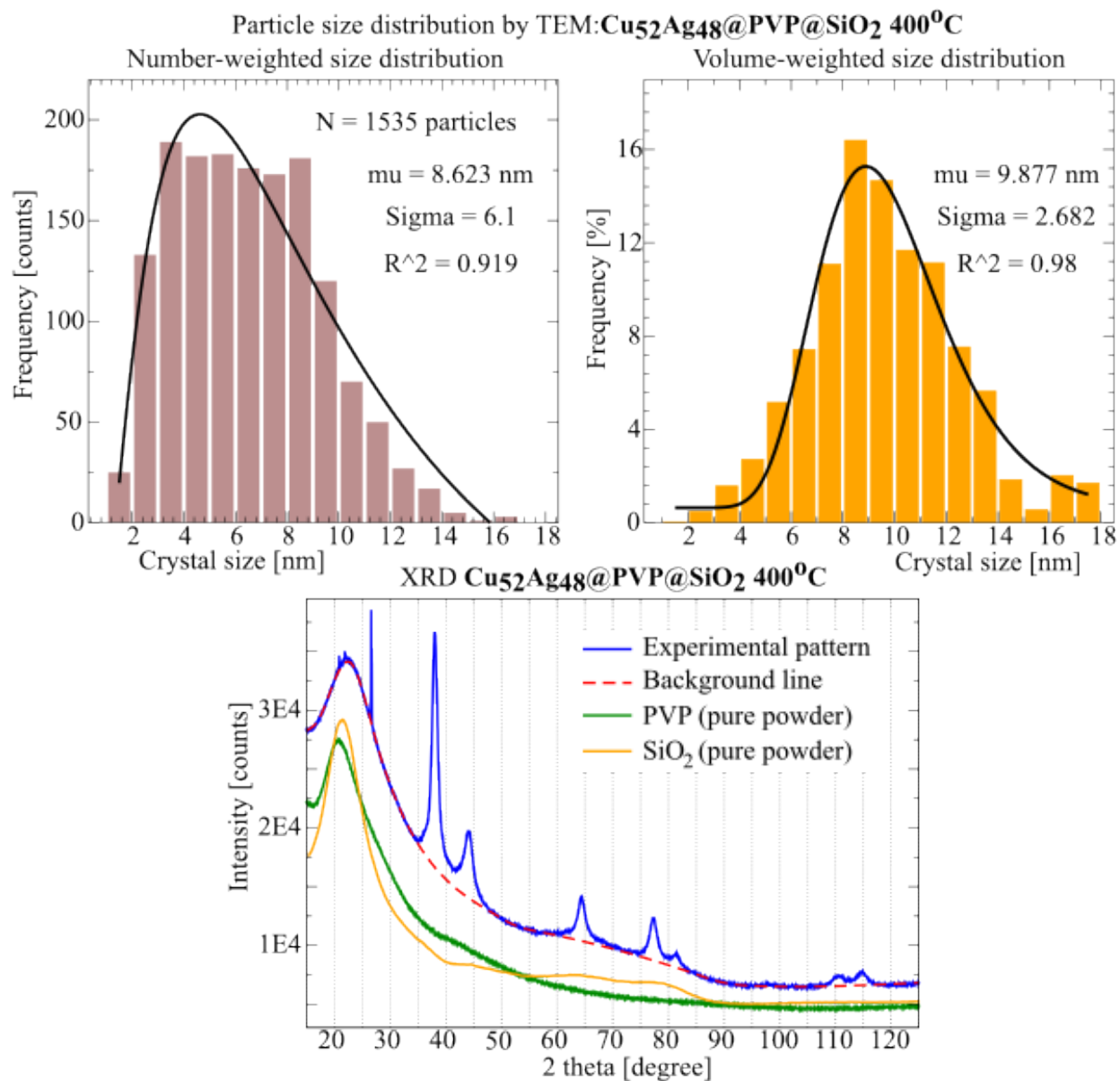


Data S 14  $\text{Ag}_{44}\text{Pt}_{56}@PVP@SiO_2$  600 °C sample analysis: TEM GSD; X-ray diffraction pattern of the experimental sample (blue line), applied background (red dotted line), and scaled diffraction pattern of the supporting material (yellow and green lines). According to the TEM EDX mapping analysis, NPs were found to be mostly in the form of an alloy.

## GROUP 6 CuAg@SiO<sub>2</sub>

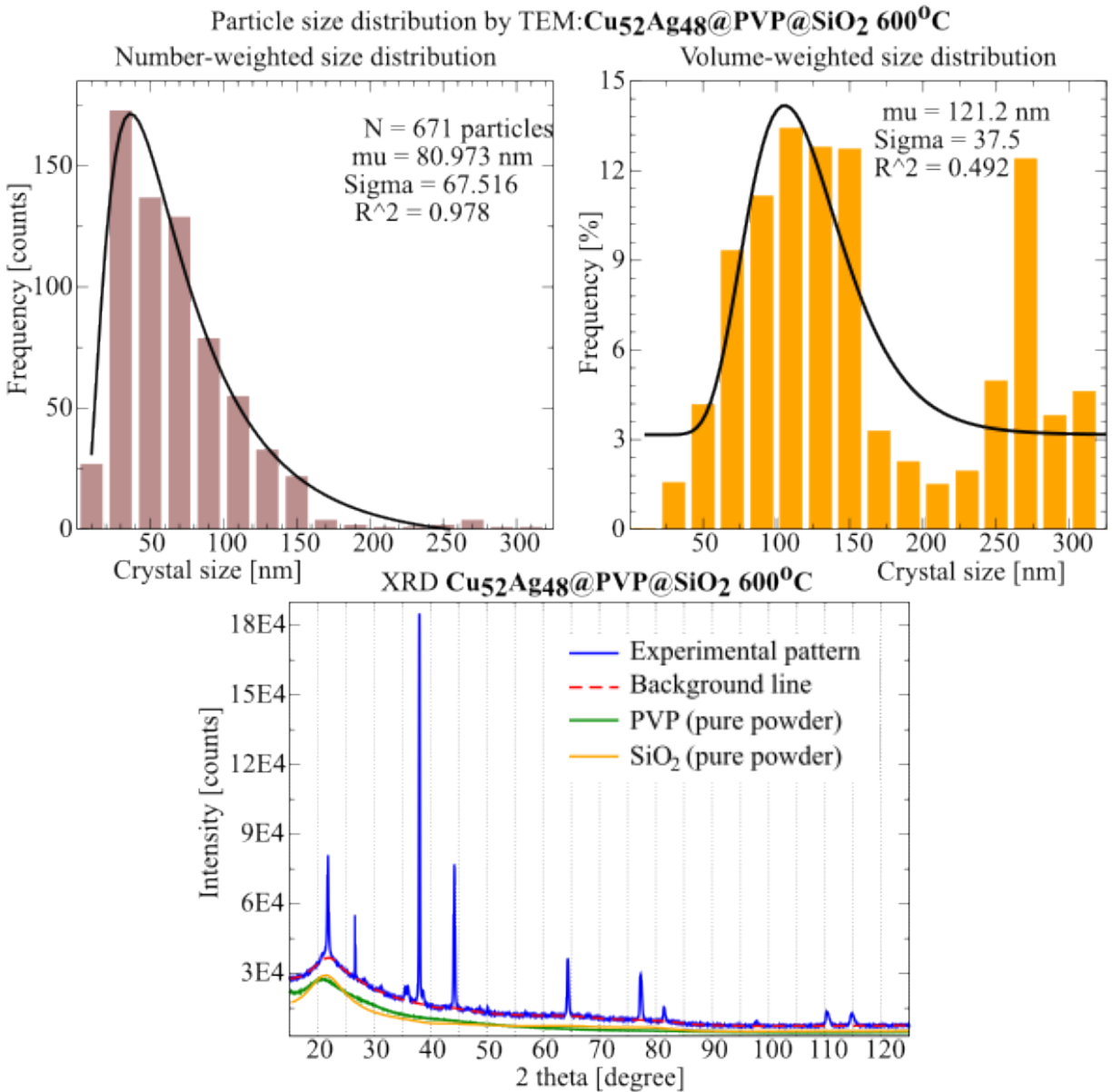


Data S 15 Cu<sub>52</sub>Ag<sub>48</sub>@PVP@SiO<sub>2</sub> RT sample analysis: TEM GSD; X-ray diffraction pattern of the experimental sample (blue line), applied background (red dotted line), and scaled diffraction pattern of the supporting material (yellow and green lines). According to the TEM EDX mapping analysis, NPs were mostly found in the form of an alloy, as well as in the form of individual Ag and Pt nanoparticles.



Data S 16 Cu<sub>52</sub>Ag<sub>48</sub>@PVP@SiO<sub>2</sub> 400 °C sample analysis: TEM GSD; X-ray diffraction pattern of the experimental sample (blue line), applied background (red dotted line), and scaled diffraction pattern of the supporting material (yellow and green lines). According to the TEM EDX mapping analysis, NPs were mostly in the form of an alloy.





Data S 17 Cu<sub>52</sub>Ag<sub>48</sub>@PVP@SiO<sub>2</sub> 600°C sample analysis: TEM GSD; X-ray diffraction pattern of the experimental sample (blue line), applied background (red dotted line), and scaled diffraction pattern of the supporting material (yellow and green lines). According to the TEM EDX mapping analysis, NPs were mostly in the form of an alloy.

## References

- 
- 1 Z. Kaszkur and I. Smirnov., arXiv:2212.06926 [*cond-mat.mtrl-sci*], 2022.
  - 2 C. L. Cleveland, U. Landman, T. G. Schaaff, M. N. Shafiqullin, P. W. Stephens and R. L. Whetten, *Phys. Rev. Lett.*, 1997, **79**, 1873–1876.
  - 3 J. Turkevich, P. C. Stevenson and J. Hillier, *Discuss Faraday Soc*, 1951, **11**, 55–75..
  - 4 K. C. Grabar, K. J. Allison, B. E. Baker, R. M. Bright, K. R. Brown, R. G. Freeman, A. P. Fox, C. D. Keating, M. D. Musick and M. J. Natan, *Langmuir*, 1996, **12**, 2353–2361.